Correspondence

Proposal for a Pulsed Ferromagnetic Microwave Generator*

The generation of microwave radiation by means of a system of spins was accomplished several years ago with the invention of the paramagnetic maser. It has been realized for some time that an analogous ferromagnetic device would have two major potential advantages: it could provide much larger amounts of power because of the larger number of spins available and because nearly all the spins rather than a fraction exp $(-\hbar\omega/kT)$ are lined up; and it could operate at room temperature.

Several schemes have been proposed and utilized[1]-[1] for such a device. In all of these, the magnetization of a saturated ferromagnet is transiently brought into a state in which it is not aligned with the magnetic field and is then made to radiate into a circuit at the free precession frequency. We are here proposing a new method for producing a nonaligned magnetization which may have some advantages.

For certain ranges of value of the crystalline anisotropy constants (which can be obtained in several known compounds of both cubic and hexagonal structure), the uniform magnetization of a saturated monocrystalline ellipsoid can assume two or more orientations. The energy is lowest in one of these orientations; the others are metastable, corresponding to local but not absolute minima of the energy surface.

The sample can be put into a metastable state by turning on a field large enough to produce an absolute energy minimum in the direction of the field. The field can then be reduced or rotated until some other direction of the magnetization becomes absolutely stable (corresponding to a deeper energy minimum). If now the field is changed further until the metastable minimum disappears, the magnetization will precess about the direction of the new (absolute) minimum and can radiate into a microwave circuit.

An example of such a process is furnished by a disc of cubic material with positive anisotropy cut parallel to a (100) plane, and thus containing four easy (100) directions. Let the sample be saturated by applying a field larger than the anisotropy field H_A along one of these directions. If the applied field H is now reduced to some value in the range $\frac{1}{4}H_A < H < H_A$, and rotated in the plane of the disc, the magnetization becomes metastable as soon as the angle of rotation exceeds 45°. At some angle of rotation between 45° and 90°, the metastable direction becomes unstable, and the magnetization

precesses about a new direction. The conditions for the instabilities and equilibria are readily computed. We can get an idea of the magnitudes involved from a numerical example; if $H = \frac{1}{2}H_A$, the instability first occurs when the angle of rotation is 55.7° and the initial departure of the magnetization from its new equilibrium orientation is 48.7°.

The radiated frequency depends on the values of H, the first- and second-order anisotropy constants K_1 and K_2, and the magnetization M, and can be computed readily. For a numerical example consider a (100) disc with a longitudinal demagnetizing factor of 0.8 (transverse demagnetizing factor 0.1) cut from a material with $4\pi M = 5000$ gauss, first-order anisotropy field $H_A = 2000$ oersteds, and $g = 2.3$. The radiated frequency varies from 8 to 12 kMc as the applied field is changed from 1700 to 1100 oersteds. The energy that is potentially available for the radiation is the difference between the metastable and final energy minima which, for this example, varies from 5×10^4 to 10^4 ergs per cubic cm over this frequency range. Assuming a 0.01-cm³ sample, a 1-μsec pulse, and an efficiency of 10 per cent, this would furnish a pulse power of 1 to 5 watts.

The constants of the material for this numerical example have been chosen from the values characteristic of dilute (approximately 20 per cent) cobalt ferrite. The main difficulty in using this substance in such an experiment is the rather large linewidth (low intrinsic Q), which implies a restriction to extremely short pulses. For a first experiment it may be easier to use the anomalous anisotropy observed in yttrium iron garnet at liquid helium temperatures.[5]

One phenomenon associated with the proposed experiment should be mentioned. It has been pointed out by Schaug-Pettersen[6] that under certain conditions a class of spinwaves in a ferromagnetic specimen can exhibit unstable growth. In the experiment proposed here, the instability of the uniform precession which we wish to exploit is always preceded by such a spinwave instability. Since the growth of spinwaves does not contribute to the microwave radiation,[6] it is necessary to traverse the spinwave instability region rapidly. Thus the applied field cannot be rotated slowly, but must be pulsed over a portion of the cycle. With the disc geometry described here the spinwave instability region can be made quite narrow and the growth rate can be kept relatively small. Exact calculation is difficult, but a rough estimate indicates that the requirements are well within the capabilities of present pulse techniques.

M. W. MULLER
Varian Associates
Palo Alto, Calif.

* Received by the IRE, March 1, 1961.
[1] R. V. Pound, "Microwave Pulse Generator," U. S. Patent No. 2,873,370; February 10, 1959.
[2] F. R. Morgenthaler, "Microwave radiation from ferrimagnetically coupled electrons in transient magnetic fields," IRE TRANS. ON MICROWAVE THEORY AND TECHNIQUES, vol. MTT-7, pp. 6–11; January, 1959.
[3] B. J. Elliott, T. Schaug-Pettersen and H. J. Shaw, "Pulsed ferrimagnetic microwave generator," *J. Appl. Phys.*, vol. 31, pp. 400S–401S; 1960.
[4] P. Wolf, *J. Appl. Phys.*; March, 1961.
[5] J. F. Dillon Jr., "Ferrimagnetic resonance in yttrium iron garnet at liquid helium temperatures," *Phys. Rev.*, vol. 111, pp. 1476–1478; September, 1958.
[6] T. Schaug-Petersen, "Growing spin waves in ferrites in unstable equilibrium," *J. Appl. Phys.*, vol. 31, pp. 382S–383S; May, 1960.

RF-Induced Negative Resistance in Junction Diodes*

Experiments in using junction diodes as harmonic generators have brought to our attention a peculiar effect in the bias circuit. It was noticed that over a region of reverse bias voltage, an increase in voltage resulted in a bias-current decrease, indicating a negative resistance. This effect existed only while the fundamental RF power was driving the diode but was present both when the power at the harmonic frequency was allowed to dissipate and when it was not.

One type of RF-induced negative resistance in junction diodes has recently been reported by Hefni.[1] However, we have observed an additional type of negative resistance in our diodes. The diodes can exhibit either of two types of negative resistance, depending on the reverse bias voltage at which the impedance of the diode is matched to the RF source. Small biases give rise to the type in which current is a multiple valued function of voltage (S type), while larger biases effect the type in which voltage is a multiple valued function of current (N type).

A circuit diagram of the experimental set-up is shown in Fig. 1. The harmonic output circuit is not shown. The RF frequency was about 350 Mc. Input power ranged from 50 to 100 mw. The oscilloscope displayed applied bias voltage on the horizontal axis and bias current on the vertical axis. The diode I-V characteristic was observed on the scope with the RF signal applied to the diode. When the matching network was correctly tuned, so that sufficient power could flow to the diode, the negative resistance characteristic appeared. Fig. 2 shows curve traces for a graded junction silicon diode (MA 4380 X) exhibiting an N-type negative resistance in Fig. 2(a) and an S-type in Fig. 2(b). It was found that both types could also be obtained with an abrupt junction diode (TIC 64).

Using the S-type negative resistance we were able to obtain astable, monostable or bistable operation of the bias circuit. In the astable mode, the period of oscillation is dictated by the time constant of the bias circuit. Output waveforms for the three modes of operation are shown in Fig. 3.

The highest frequency at which the circuit will oscillate should be limited primarily by the driving frequency because of the mechanism which is proposed to explain the negative resistance. The phenomenon of hole storage is proposed as the cause, but a current change in the bias circuit should require at least one cycle of the driving signal and may require many cycles. We are trying to develop a theory which will predict the negative resistance and establish frequency limitations.

* Received by the IRE, March 1, 1961.
[1] I. Hefni, "Effect of minority carriers on the dynamic characteristic of parametric diodes," *Electronic Engrg.*, vol. 32, pp. 226–227; April, 1960.
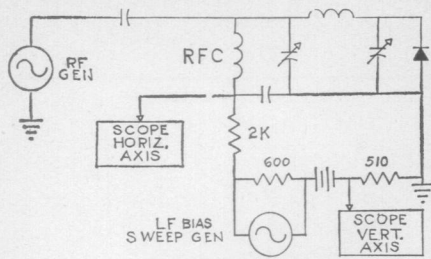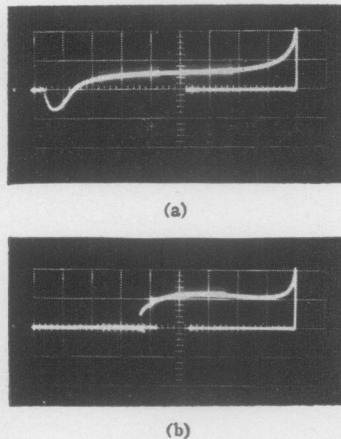
Fig. 1.—Circuit diagram.

Fig. 2.—I-V Characteristics showing (a) *N*-type and (b) *S*-type negative resistance in a MA 4380 X diode. The I-V characteristic with power off is also shown. Horizontal scale: 2 v/cm, increasing to the right. Vertical scale: 0.5 ma/cm, positive upward.
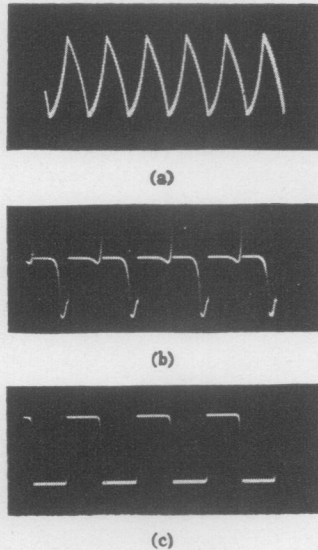

Fig. 3—Output waveforms of the bias circuit in (a) astable, (b) monostable, and (c) bistable operation. The output is about 1 v peak to peak and was taken across the 510-Ω resistor in the bias circuit. The load lines were determined by the bias voltage and the total resistance of the bias circuit. The astable frequency was 100 kc. The monostable and bistable outputs were triggered by pulses at 2 kc.

Fig. 4 exhibits two interesting features of a diode biased near zero. The first is the appearance of an additional *N*-type negative resistance close to zero bias. The second is that this additional negative resistance disappears when the harmonic power is drawn from the diode.
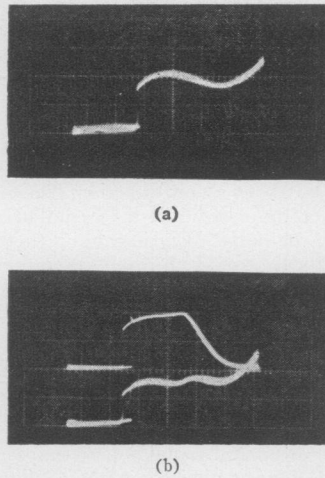

Fig. 4—(a) Negative resistance of a TI C 64 diode near zero bias. Horizontal scale: 3 v/cm centered at −6 v. Vertical scale: 0.3 ma/cm. (b) The lower curve shows cancelling of the negative resistance due to power being drawn at five times the input frequency. The upper curve shows power output vs bias voltage. Peak output is 5 mw at −5.5 v bias. Input was 50 mw at 350 Mc.

This negative resistance near zero bias is similar in appearance to an RF-induced negative resistance observed by North on welded contact diodes.[2] Capacitance variation with voltage was proposed to explain North's negative resistance. It seems reasonable that the negative resistance should disappear when harmonic power is drawn from the diode because this has the effect of adding positive resistance to the diode.

The helpful advice of I. Friedberg on this work is gratefully acknowledged.

JAMES C. MCDADE
Diamond Ordnance Fuze Labs.
Washington 25, D. C.

[2] H. C. Torrey and C. A. Whitmer, "Crystal Rectifiers," M.I.T. Rad. Lab. Ser., McGraw-Hill Book Co., Inc., New York, N. Y., vol. 15, p. 401; 1948.

Note on Coherence vs Narrow-bandedness in Regenerative Oscillators, Masers, Lasers, etc.*

In several discussions with engineers and physicists engaged in pushing the art of generating coherent radiation to shorter wavelengths, I have noted that the narrow-bandedness of the radiation produced, if not confused with the coherence[1] of this radiation, is often considered to be a measure of the degree of coherence. I would like to point out that coherence is not a quantitative concept, but a qualitative one; either radiation is coherent, or it is not, regardless of bandwidth considerations. If the duration

[1] The term "coherence" is used here in the sense of CW radiation which can interfere with indefinitely delayed portions of itself. It should not be confused with optical coherence, which refers to the property which two light beams have of interfering with each other when they are obtained from a common source.

of the signal is not indefinite, due to physical limitations such as the heating of a ruby laser, or of the source of pumping radiation, either the radiation is coherent during its ephemeral duration, or it is not.

Theoretical experiments, probably realizable at later times, may be useful to form a picture of the concept involved here.

Consider a source of narrow-banded radiation which must be tested for coherence, and designate its approximate center frequency by f. If the source output is heterodyned with two assumedly available perfectly monochromatic signals proportional to $\cos 2\pi ft$ and $\sin 2\pi ft$ respectively, the two components of a phasor are obtained.

The behavior of this phasor will constitute the criterion of coherence vs noncoherence of the radiation studied.

If this radiation is incoherent, the phasor end will be observed to execute a two-dimensional random walk at a rate inversely proportional to the bandwidth of this radiation, and if the experiment is continued over a sufficiently long period of time, the statistical location of this phasor end will be describable by a probability distribution which, in most instances, will be a Gaussian "mole-hill" centered at the origin [Fig. 1(a)].
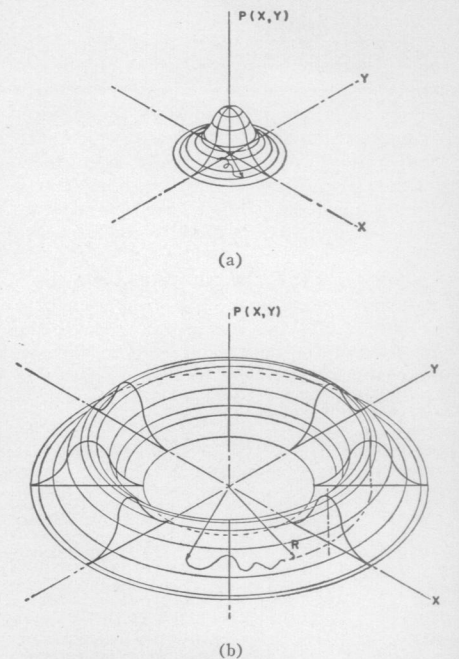

Fig. 1—Probability distribution of the phasor representing the relationship between a narrow-band signal and a perfectly monochromatic reference signal, for two cases. (a) The signal is incoherent. The distribution is a "mole-hill" centered on the origin, showing no tendency toward regulation of amplitude. (b) The signal is coherent. The "mole-run" distribution shows strong tendency to regulate amplitude to the value R but substantial random drift in phase may occur.

Superimposed on the random walk of the phasor end, there will be a circular drift proportional to the departure of f from the exact center frequency of the source spectrum.

On the other hand, if the radiation studied is coherent, the phasor end will be observed to execute a random walk statistically describable by a probability distribution

which, in most instances, will be a circular "mole-run" centered at the origin, but with vanishingly small probability at that origin [Fig. 1(b)]. Any radial cross section of this mole-run will, in general, be approximately Gaussian. Radial excursions of the phasor end away from the center circle of the mole-run will resemble the excursions about zero of the thermal voltage on a condenser shunted by a resistance, for the regenerative property of the oscillator will tend to maintain constant the average length of the phasor. Conversely, circumferential excursions of the phasor end will assume the character of a random walk, the rate of which has been calculated in a former article.[2] A slow average rotation will be superimposed on this circumferential random walk, the rate of this rotation being proportional to the departure of f from the exact center frequency of the source spectrum.

It is essential to note that there is no fixed phase reference to which the phasor may be brought back with a restoring force proportional to the departure of the phasor from this phase reference. Thus, a probability distribution of the phasor end describable by a mole-hill at a distance from the origin (Fig. 2) is fundamentally impossible.
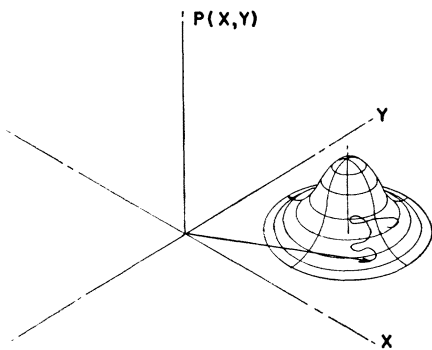

Fig. 2—This probability distribution is not a possible result in the limit as observation time approaches infinity since it would imply "phase-locking" with the hypothetical reference signal.

Experimental verification of the phasor's behavior for laser's outputs has not been obtained, but it may be speculated that when the radiation from two relatively stable lasers is caused to interfere on two photocells, with a quarter-wave difference between the two path differences from the two lasers to the two photocells, the photocells' outputs will represent a phasor, the phase of which is the phase difference of the two lasers. Whether or not the character of the probability distribution of the phasor end can be detected in such an experiment will depend upon whether the bandpass of the photocells' outputs exceeds or does not exceed the instantaneous frequency difference of the two lasers.

M. J. E. GOLAY
The Perkin-Elmer Corp.
Norfolk, Conn.

[2] M. J. E. Golay, "Monochromaticity and noise in a regenerative electrical oscillator," PROC. IRE, vol. 48, pp. 1473–1477; August, 1960.

Note on the Probable Character of Intelligent Radio Signals from Other Planetary Systems*

Experiments are now being planned[1] to detect radio messages aimed at the earth from planets of other solar systems—experiments which few believe will succeed, but which few would not want to see tried.

The spectral location, as well as the character of these signals, constitute subjects for stimulating speculation.

It may well be surmised that these hypothetic signals will have a spectral location related in a simple manner to the 1421-Mc line of hydrogen, and since this line is located in a relatively noisy region of the cosmic radio spectrum, a location at either half or at twice its frequency appears fairly probable.

It may be surmised further that these signals will contain a coherent component[2] at as nearly half or twice the hydrogen frequency as available accuracy permits. Following this line of reasoning, we may expect the senders to correct this frequency for the component of motion of their transmitter in the direction of transmission with respect to the center of gravity of their planetary system, as well as for the gravitational potential of that transmitter with respect to their "local" outer space; corrections which we should also make for our receiver.

Even when so corrected, the coherent signal postulated here will have to be further corrected for the nebular drift between the two solar systems, unless of course it is already corrected at the transmitting end. Thus, it would appear that there may be four likely spectral regions within which a search should be made for coherent signals, before any intelligent messages can be received: at half or at twice the hydrogen frequency, and with or without correction for nebular drift.

The extent of each search region will be determined mostly by our—or their—uncertainty in nebular drift, and to a lesser extent by the relative error of sender and receiver in determining the exact hydrogen frequency or the various corrections indicated above. It must be noted that the two search regions at half the hydrogen frequency are only a quarter as wide as the two search regions at twice that frequency and that this factor of four is exactly compensated by the four-fold smaller directivity of a reflector of a given size at the lower frequency. When such factors as easier power generation and greater space coverage are considered, the two half-frequency regions appear more favorable.

The bandwidth of search, Δf, within each region is a matter for much conjecture, but once this bandwidth has been decided upon, the manner of search appears straightforward. The signals received are heterodyned with $\cos 2\pi ft$ and $\sin 2\pi ft$, respectively, where f designates a frequency within the search region, and the two outputs are filtered by two low-pass RC filters with a

time constant of the order of

$$RC = \frac{1}{\pi \Delta f}.$$

The filter outputs constitute the two components of a phasor, the behavior of the end of which should be studied for a time equal to a few times the time constant of the dual low-pass filters. If a "mole-run" tendency is detected for the statistical distribution of the phasor end, and if this tendency is confirmed by extending the time of search, the presence of intelligent transmission within the $f \pm \Delta f/2$ region will be ascertained with a probability of error which decreases exponentially with time.

Since, for a given transmitting power, the bandwidth of search Δf decreases with the inverse square of the distance, and since the time required for searching a given region increases with the inverse square of Δf, the fourth power law relating total time of search and distance will require that several Δf-wide regions be searched simultaneously, in order to cover the total search regions in a reasonable time.

It is of interest to note the basic difference between the search procedure outlined above, and the search procedure which consists in recording a narrow spectral region, forming the auto-correlation function of the recorded signals, and taking the Fourier transform in cosines of this auto-correlation function. This latter method serves to reveal the presence of extra spectral energy within narrow bands, but does not preserve phase information. Thus, a coherent signal which is slightly phase modulated becomes indistinguishable from a spectral line with a width equal to the frequency excursion, whereas the mole-run character of the phasor-end statistical distribution which can be detected with the method discussed above serves to establish with increasing certainty that coherent signals are indeed coherent.

M. J. E. GOLAY
The Perkin-Elmer Corp.
Norwalk, Conn.

VHF Satellite Signals Received at Extra Optical Distances*

Smyth Research Associates have been conducting an experimental program on low angle refraction of radio waves penetrating the atmosphere. Satellite transmitters at 108, 162, and 216 Mc have been used as signal sources in these studies. During the course of the measurements (June, July and August, 1960), it was found that on the majority of passes, signals were received while the satellite was well beyond the radio horizon. Out of a total of 49 cases when such "precursor" signals were sought, only 14 failed to yield signals for at least one minute beyond the radio horizon.

In two cases, signals were first received when the satellite was 1700–1900 miles beyond the radio horizon point at orbit height. On these passes the satellite was roughly twice as far away as the distance to the horizon. The signal strength on these occasions was 11 db below the free space level on 216 Mc and 18 db below the free space level on 108 Mc. As can be seen in Fig. 1, there ap-
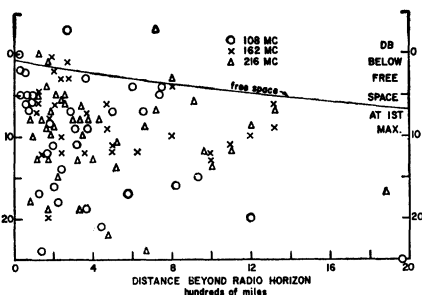

Fig. 1—Precursor signal levels.

pears to be no distinct dependence of received signal strength on frequency. Even simultaneous data on 162 and 216 Mc show no consistent frequency dependence.

The combination of low attenuation and no frequency dependence suggests a tropospheric ducting mechanism. Correlation of local radiosonde data with signal strength and maximum path length supports this view. The duct thickness and intensity in all cases when signals were observed, exceeded the trapping requirements for frequencies above 100 Mc.
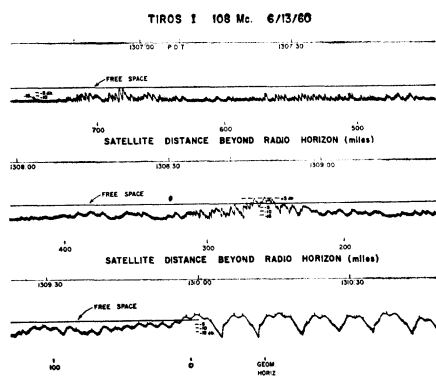
Fig. 2 shows the data record for one of

Fig. 2—Satellite precursor signals.

these cases, together with a scale of the great circle distance of the satellite below the radio horizon. The record was taken at the SRA Point Buchon field site on the coastline near San Luis Obispo, California, with a sea-interferometer system, giving rise to the pattern of maxima and minima above the horizon. Relatively minor tumbling nulls can also be seen superimposed on the interferometer trace.

LLOYD J. ANDERSON
Smyth Res. Associates
San Diego, Calif.

WWV and WWVH Standard Frequency and Time Transmissions*

The frequencies of the National Bureau of Standards radio stations WWV and WWVH are kept in agreement with respect to each other and have been maintained as constant as possible with respect to an improved United States Frequency Standard (USFS) since December 1, 1957.

The nominal broadcast frequencies should, for the purpose of highly accurate scientific measurements, or of establishing high uniformity among frequencies, or for removing unavoidable variations in the broadcast frequencies, be corrected to the value of the USFS, as indicated in the table. The corrections reported have been improved by a factor of three over those previously reported, by means of improved measurement methods based on LF and VLF transmissions.

The characteristics of the USFS, and its relation to time scales such as ET and UT2, have been described,[1] to which the reader is referred for a complete discussion.

The WWV and WWVH time signals are also kept in agreement with each other. Also they are locked to the nominal frequency of the transmissions and consequently may depart continuously from UT2. Corrections are determined and published by the U. S. Naval Observatory. The broadcast signals are maintained in close agreement with UT2 by properly offsetting the broadcast frequency from the USFS at the beginning of each year when necessary. This new system was commenced on January 1, 1960. A retardation time adjustment of 20 msec was made on December 16, 1959; another retardation adjustment of 5 msec was made at 0000 UT on January 1, 1961.

WWV FREQUENCY
WITH RESPECT TO U. S. FREQUENCY STANDARD

1961 February	Parts in 10^{10}[†]
1	−150.7
2	−150.4
3	−150.5
4	−150.8
5	−150.9
6	−151.0
7	−151.1
8	−150.5
9	−149.8
10	−149.6
11[‡]	−148.0
12	−149.3
13	−149.6
14	−150.0
15	−150.1
16	−150.4
17	−150.7
18	−150.9
19	−150.8
20	−150.6
21	−150.5
22	−150.2
23	−150.2
24	−150.3
25	−150.4
26	−150.2
27	−150.3
28	−150.1

† A minus sign indicates that the broadcast frequency was low. The uncertainty associated with these values is $\pm 5 \times 10^{-11}$.

‡ The frequency was decreased 1×10^{-10} on February 11, 1961.

NATIONAL BUREAU OF STANDARDS
Boulder, Colo.

[1] "National Standards of Time and Frequency in the United States," PROC. IRE, vol. 48, pp. 105–106; January, 1960.

A Ruby Laser with an Elliptic Configuration*

A ruby laser with a new configuration was successfully operated at 1/15 input threshold energy of previous lasers.[1,2] This decrease in pump energy was accomplished by a new configuration which efficiently focuses the pump radiation into the ruby rod.

The laser is an optical maser[3] and is the only known device which can produce highly coherent radiation in the optical region. Fig. 1 shows details of the new device. Its most important elements are the specially processed ruby, the high-intensity discharge lamp which produces the pump power, and the cylindrical ellipse reflector which focuses the pump power into the ruby rod
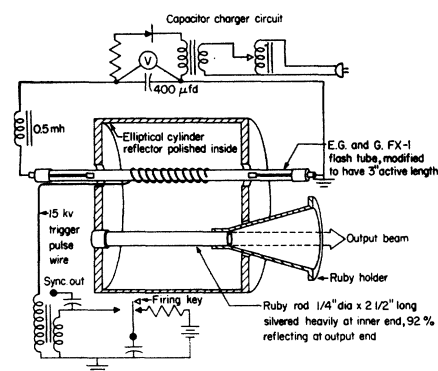

Fig. 1—Schematic of optical maser with elliptical reflector.

The ruby is an Al_2O_3 crystal with chromium atoms replacing some of the aluminum atoms. A ruby which was 0.05 per cent Cr_2O_3 by weight was used. The end planes of the ruby rod are flat to a fraction of a micron and parallel to within 50×10^{-6} inch.

The ruby laser has a high-energy pump power requirement. For the efficient use of the pump radiation a focusing system must concentrate the pump energy into the ruby, and must do it without the radiation passing through the lamp since an emission lamp is an absorbing medium. This can be achieved with an elliptical cylinder configuration with the lamp along one focal line and the ruby along the other. In order to have sufficient gain per reflection, a *long* cylindrical ruby is used to offset losses inherent in the reflecting coatings. Therefore, a *cylindrical* ellipse is a good configuration. The new laser was operated at 150 joules threshold pump energy as opposed to the 2300 joules previously required.

This configuration has other advantages. Cooling of either the ruby or the lamp or both can be achieved in a variety of ways,

[1] T. H. Maiman, "Stimulated optical radiation in ruby," *Nature*, vol. 187, pp. 493–496; August, 1960.
[2] R. J. Collins, D. F. Nelson, A. L. Schawlow, W. Bond, C. G. B. Garrett, and W. Kaiser, "Coherence, narrowing, directionality, and relaxation oscillations in the light emission from ruby," *Phys. Rev. Letters*, vol. 5, pp. 303–305; October, 1960.
[3] J. R. Singer, "Masers," John Wiley and Sons, Inc., New York, N. Y.; 1959.

such as circulating a coolant or using filters on the reflector walls or along the minor axis of the ellipse to protect the ruby from unwanted pump radiation. A cryostat can be used outside the elliptic cylinder to cool the ruby. Thus, continuous (CW) operation of this laser configuration may become feasible if sufficiently intense light sources can be found. Other details are given in Fig. 1.

Fig. 2 shows the energy levels and associated parameters of the chromium atoms in Al_2O_3 pertinent to the laser. These atoms are excited to the $^4F_2$ level by the radiation from the discharge lamp. For the production of coherent radiation ("laser-action"), it is
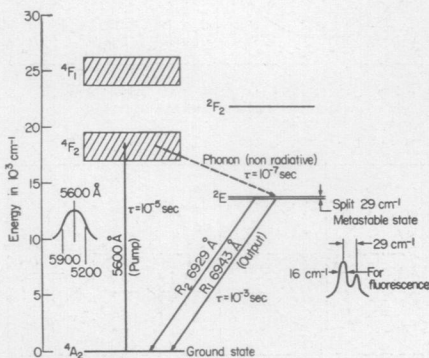
Fig. 2—Energy-level diagram of ruby.

necessary to highly overpopulate the ^2E metastable state. This is feasible primarily because of the broad energy width of the $^4F_2$ level and the large-lifetime τ_{21} compared to τ_{32}. The $^4F_2$ level is only one of several levels involved from which the atoms may decay to the metastable state.

Fig. 3 shows synchroscope pictures of the laser output vs time as a function of input
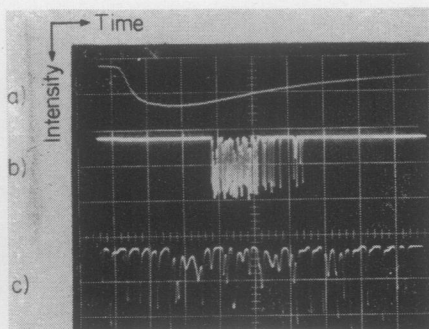

Fig. 3—(a) Fluorescence when input is 144 joules, gain 500, sweep 100 μsec/cm. (b) Laser output when input is 222 joules, gain 1, sweep 100 μsec/cm. (c) Laser output when input is 222 joules, gain 1, sweep 10 μsec/cm delayed 360 μsec from start of flash.

energy. At threshold input energy for laser action, the output radiation forms a parallel beam which produces a highly concentrated bright spot on the screen. The output radiation below threshold input energy comes from spontaneous emission and spreads in all directions and is barely visible. Further experiments are in progress to investigate the

mechanism of the pulses[4] shown in Fig. 3(c). The energy bandwidth of the laser output as measured with a Fabry-Perot interferometer was found to be in the vicinity of 0.06 cm^{-1}. The details of these measurements will be reported later.

A self-contained portable version of this new laser has been constructed and weighs only 19 pounds, including the transistorized battery-operated power supply.

M. Ciftan
Microwave and Power Tube Division
C. F. Luck
C. G. Shafer
H. Statz
Research Division
Raytheon Company
Waltham, Mass.

[4] H. Statz and G. deMars, "Transients and oscillation pulses in Masers," in "Quantum Electronics Symposium," C. H. Townes, Ed., Columbia University Press, New York, N. Y.; 1940.

C-Band Nondegenerate Parametric Amplifier with 500-Mc Bandwidth*

A *C*-band nondegenerate parametric amplifier has been developed that has the following characteristics:

Signal frequency:	5.3 kMc
Idler frequency:	9 kMc
Pump frequency:	14.3 kMc
Instantaneous bandwidth:	500 Mc
Gain:	10 db
Noise figure:	3 db (including circulator loss).

A schematic diagram of the amplifier, which uses two commercially available silicon pill varactor diodes in a balanced circuit configuration, is shown in Fig. 1.

To obtain a large gain-bandwidth product simultaneously with a low noise figure and good operational stability, a circulator is used to interconnect the antenna, amplifier and post-receiver. Transformer T_1 changes the characteristic impedance of the circulator to the lower value required to obtain the necessary gain and bandwidth. The two varactor diodes are effectively in parallel in the signal circuit, and inductance L_s resonates with their net capacitance at the signal frequency. The parallel L-C combination in the signal circuit is used only when a double-tuned response is desired.

The equivalent idler circuit consists essentially of the two varactor diodes in series, since very little idler power flows in the signal circuit (because of the balanced circuit configuration) or in the pump circuit (because the pump power is applied through a high-pass filter). The zero-bias capacitances of the two diodes are matched within about 10 per cent, and each diode with its

associated parasitic reactance is very nearly self-resonant at the idler frequency of 9 kMc. Thus, the idler circuit bandwidth is about the widest obtainable without additional resistive loading (which would degrade the amplifier noise performance).
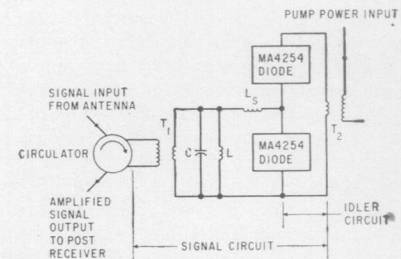

Fig. 1—Schematic diagram of *C*-band nondegenerate parametric amplifier.

Fig. 2 shows the measured gain-frequency characteristic of the amplifier under single-tuned conditions. As shown, a bandwidth of 500 Mc and a peak gain of 10 db are obtained. The noise figure of the amplifier-circulator combination is 3 db at the midband frequency of 5.3 kMc. The noise figure varies over the pass-band by about ± 0.5 db, being lower below midband frequency and higher above midband frequency mainly because of the changing ratio of signal-to-idler frequencies.
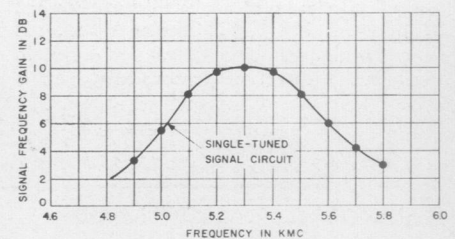

Fig. 2—Measured gain characteristic of C-band nondegenerate parametric amplifier.

The diodes are operated at zero bias and require a total pump power of about 130 mw. The amplifier gain varies by only ± 0.5 db for a ± 1-db change in pump power and is very insensitive to antenna, post receiver, or circulator impedance variations. Two of the single-tuned amplifier-circulator combinations can readily be cascaded to provide 20-db gain with an over-all bandwidth of 350 Mc; even wider bandwidths are possible with the same peak gain if the tuning of the amplifiers is slightly staggered. Further theoretical and experimental work is presently in progress to obtain much wider amplification bandwidths through the use of double-tuned signal and idler circuits.

J. Kliphuis
Airborne Instruments Lab.
Melville, N. Y.

Backward-Wave Radiation from Periodic Structures and Application to the Design of Frequency-Independent Antennas*

One characteristic common to a large number of successful frequency-independent log-periodic and log-spiral antennas is that the radiation is directed toward the apex or feed point of the structure.[1-3] In attempting to explain this property, and more generally to understand the operation of log-periodic antennas, it was found useful to think of the antenna as a locally periodic structure whose period varies slowly, increasing linearly with the distance to the apex.

It is well known that a number of diffracted beams are produced when a plane wave is diffracted by an infinite plane grating. Each beam corresponds to a space harmonic which has a phase constant $\beta_n = \beta_0 - (2n\pi/a)$ along the grating where a is the period of the grating. The wave characterized by β_0 is the fundamental wave. The same description applies to a wave guided along the grating and having a phase constant β_0 in that direction. For example, Fig. 1 shows a dielectric slab bounded on one side by a conductor and on the other side by a grating. If this supports a slow wave ($\beta_0 > k = \omega\sqrt{\mu\epsilon}$) and if the period a is small, $p = 2\pi/a$ will be large and all the $\beta_n = \beta_0 - np$ (for n positive or negative integer) will be larger than k. None of the diffracted beams has a real direction of propagation which means that no radiation occurs for the infinite structure. If now the spacing is increased, p will become smaller, the point β_1 (and all the points β_n) will move toward β_0 and eventually β_1 will become less than k. When this happens, the diffraction occurs in the negative direction (backward wave). If
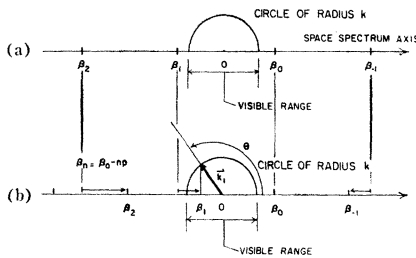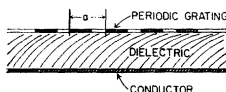

Fig. 1—(a) When a is small, $p = 2\pi/a$ is large, no radiation occurs. (b) When a increases, the points β_n move as indicated. In the case shown here, one wave is in the visible range.

[1] D. E. Isbell, "Non-Planar Logarithmically Periodic Antenna Structures," Antenna Lab., Univ. of Illinois, Urbana, Tech. Rept. No. 30, Contract AF33 (616)-3220; February, 1958.
[2] R. H. DuHamel and F. R. Ore, "Logarithmically periodic antenna designs," 1958 IRE NATIONAL CONVENTION RECORD, pt. 1, pp. 139–151.
[3] J. D. Dyson, "The unidirectional equiangular spiral antenna," IRE TRANS. ON ANTENNAS AND PROPAGATION, vol. AP-7, pp. 329–334; October, 1959. Also, Antenna Lab., Univ. of Illinois, Urbana, Tech. Rept. No. 33, Contract No. AF33 (616)-3220; July, 1958.

the spacing is further increased the points β_2, then β_3, and so on will enter the circle of radius k and several beams can result, radiated at angles from the z direction which may be obtained from the construction shown in Fig. 1.

$$\cos\theta_n = \frac{\beta_n}{k} \quad (|\beta_n| < k).$$

The increase in spacing may occur progressively along a single structure as in a log-periodic grating. As the fundamental wave progresses, it will successively reach points where the various conditions outlined above will occur. If the rate of increase is slow, a section of the structure about these points will behave as if it were periodic with the local period. As the fundamental wave reaches a radiation region, it will naturally be attenuated (because of this radiation) and the local value of β_0 may also be somewhat modified by this loading of the transmission medium. If the coupling is strong enough and if the detail design of the structure favors the backward wave, the radiation will cause attenuation of the fundamental wave such as to remove all the incident energy before the conditions for this radiation change too radically. The pattern will be approximately that of the periodic structure having the local value of the period. When the frequency is increased, the region where backward-wave radiation occurs (active region) will move but the pattern will be substantially the same.

These considerations have been applied and tested on periodic zig-zag and helical wires. The phase delay of the fundamental wave is approximately given by the phase constant, $\beta_0 = k \csc \gamma$, $\gamma =$ pitch angle. A zig-zag antenna was constructed which, according to the theory, should radiate in the backfire direction at 1500 Mc. Below this frequency, additional gain would be expected due to excess phase shift between cells. Above this frequency, the maximum radiation should scan away from backfire. The measured patterns are shown in Fig. 2. The same tests were made on a bifilar helix and similar results were obtained. The zig-zag and helical antennas operating in the backfire mode have smaller cross sections in terms of the wavelength than the conventional endfire zig-zag and helical antennas.

A number of new backward-wave structures are now proposed following the foregoing basic considerations. For example, a periodic monopole array over ground may be fed from a helical delay line. Typical radiation patterns of this type of periodic structure are shown in Fig. 3. The correspondence between the measured patterns and the predictions of the simple theory is good. The achievement of backward-wave radiation from an array of slots in a ground plane depends upon obtaining the proper slow phase velocity in a waveguide or line used to excite the slots. The coaxial guide with a helical center conductor seems most likely to operate satisfactorily.

The analysis and design of frequency-independent antennas of both the log-periodic and log-spiral geometries is now underway using the foregoing principles. The design procedure is to first study, either theoretically or experimentally, a periodic structure made of the same elements. The
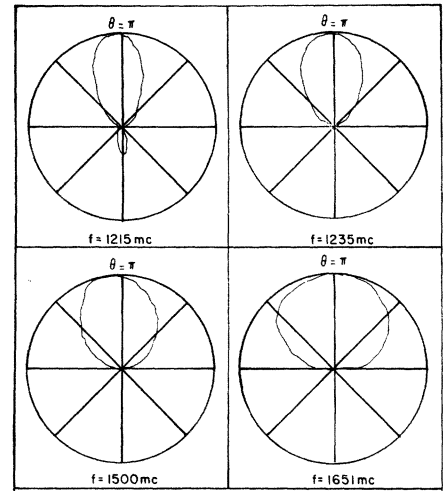

Fig. 2—E-plane radiation patterns of a backward-wave bifilar zig-zag antenna.
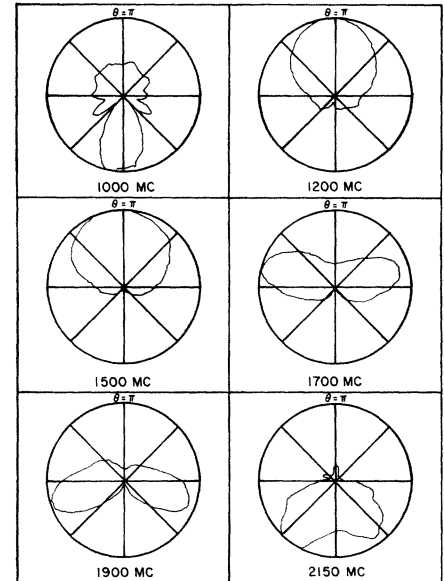

Fig. 3—H-plane radiation patterns of a periodic monopole array.

frequency-independent design is then obtained from the periodic antenna by applying a linear taper, producing a log-periodic structure. The backward-wave bifilar helix is the periodic counterpart of the conical log-spiral antenna; the backward-wave zig-zag of the log-periodic zig-zag. Similarly, backward-wave periodic dipole, monopole and slot arrays may be converted into frequency-independent antennas by a linear taper.

The importance of these observations lies not only in the understanding that they contribute to the operation of frequency-independent antennas, but also in the new structures that they suggest. The basic ingredients for a frequency-independent antenna are a slow-wave transmission medium and a series of radiating elements satisfying the similarity condition and coupled to the transmission medium at points spaced in geometric progression. Proper design can produce a wave substantially radiated toward the feed point.

Backward-wave periodic structures without tapering are antennas which deserve at-

tention for their own sake. The models which have been studied experimentally show very low sidelobes, high front-to-back ratio, and good bandwidth. Furthermore, the production of radiating waves from a periodic structure which is directly excited from a modulated electron beam appears to be a promising approach to the generation of microwave radiation.

P. E. MAYES
G. A. DESCHAMPS
W. T. PATTON
Antenna Lab.
University of Illinois
Urbana, Ill.

K_a-Band Ferrite Amplifier*

A ferrite parametric amplifier has been built and operated at a signal frequency of 20.5 kMc. It is believed that this is the highest frequency of operation of any ferrite parametric amplifier. The amplifier was operated with a pump power as low as 4 watts peak.

The amplifier used longitudinal pumping as suggested by Denton.[1] It consists of a signal cavity tunable by means of a sliding short coupled to a pump cavity also provided with a sliding short. Iris coupling was provided between the two cavities as well as between each cavity and its respective input guide. The two cavities are so arranged that the transverse field in the pump cavity (for the dominant mode) is perpendicular to the H plane in the signal cavity and thus to both transverse and longitudinal fields. The ferrite sample used was a highly polished single-crystal YIG sphere, 0.149 inch in diameter placed in the coupling region between the two cavities. A dc magnetic field was applied parallel to the transverse pump field and adjusted to resonance at the idle frequency. The rest of the microwave circuitry was conventional for one-port ferrite amplifiers and included an EH tuner in the pump line for impedance matching, a means of adjusting pump power level, band-pass filters in the signal line to block the pump power, and directional couplers for observation of reflected signal power and incident pump power. The pump power was obtained from a Microwave Associates MA210B magnetron operating at 34.8 kMc with a pulse duration of one microsecond. A 1000-cps square-wave amplitude modulated signal was used and when reflections were observed on a nonsynchronized oscilloscope two traces were displayed, one corresponding to periods with no signal input and the other corresponding to periods with a signal input. Since the pump, and therefore the amplifier,

was pulsed, one picture of the oscilloscope face gave the amplifier response with and without signal and with and without pump. Measurements of net gain were obtained by comparing the output amplitude to a reference level obtained by replacing the amplifier with a short circuit. The amplifier output was attenuated sufficiently to match this reference level and the gain read directly from the attenuator.

The YIG sphere used was large enough so that many magnetostatic modes were capable of direct excitation. Because of propagation effects in the large sphere several distinct modes were observable in which there was negligible overlap. These are the modes which are most attractive for amplification. The idle mode was a magnetostatic mode near the bottom of the magnetostatic mode spectrum. The signal mode was a quasi-magnetostatic mode; that is, it was a ferrite mode with properties similar to magnetostatic modes but it lay outside the magnetostatic mode spectrum by about 4.5 kMc.

Experimental results with this amplifier are shown in Figs. 1 and 2. In Fig. 1, gain is plotted vs signal input power level, showing gain saturation for about one watt peak power output. In Fig. 2, small signal gain is plotted vs pump power. It is seen that with a pump power as low as 5 watts peak, a net gain of 10 db is obtained. It appears that gain drops to zero for a pump power of of 4 watts. However, the impedance matching used at the pump frequency was relatively inefficient, partly because of space

Fig. 1—K-band ferrite amplifier gain curves showing gain saturation.

Fig. 2—Gain vs pump power for K-band ferrite amplifier.

limitations imposed by the large electromagnet used to furnish the dc field. It is anticipated that this threshold pump power can be reduced by several db with improvements in the matching structure.

No attempt was made to measure the noise figure of this amplifier since the magnetron pump source contributed considerable excess noise and the amplifier stability was relatively poor. It is anticipated that improvements in the pump circuit efficiency will allow the use of a klystron source, at least on a pulsed basis. Such improvements are presently being planned and noise figure measurements will then be made.

ROY W. ROBERTS
Res. Dept.
Melabs
Palo Alto, Calif.

Equivalent Circuits for a Thermoelectric Converter*

When a thermoelectric converter is operated with constant heat input rather than at a constant temperature differential, new equivalent circuits are required to explain observed effects, particularly the transient response to step function disturbances. The dynamic behavior of a lightly loaded converter—such as might be used as a power supply for tunnel diodes—can be adequately described by a thermal statement that ignores Joulean heating, as well as the Thomson effect:

$$Q = (K + K_L)\Delta T + \Pi I$$
$$+ C_H \frac{d(\Delta T)}{dt} \cdots \text{[watts]}. \quad (1)$$

This is essentially a linear, nodal equation in which the time-dependent term is the heat flowing into or out of the heat capacitance C_H (watt-seconds per degree) as the result of any variation in the temperature, ΔT. Heat losses external to the thermoelements are represented by K_L added to the internal conductance K. The cold junctions are assumed to be held at a fixed temperature by an infinite heat sink, with respect to which the temperature ΔT of the hot junction is measured.

The physical model to which (1) applies is shown in Fig. 1, but if the Peltier heat ΠI is rewritten as $K_\pi \Delta T$ where $K_\pi = \Pi S (K +R_L)^{-1}$, the revised equation then applies directly to the circuit of Fig. 2. The steady-state response of the nodal temperature ΔT to a sinusoidal excitation $Q = Q_0 \cos \omega t$ is given by

$$\Delta T = \frac{Q_0}{K_\pi + K + K_L} R_e \left[\frac{\exp j\omega t}{1 + j\omega \tau} \right]$$

where

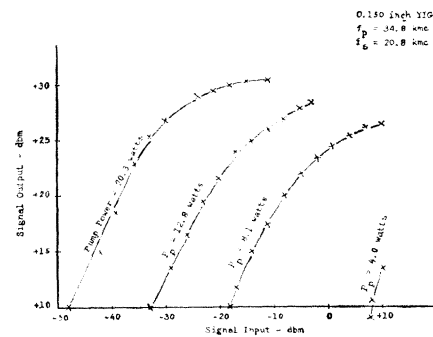$$\tau = C_H (K_\pi + K + K_L)^{-1} \cdots \text{[sec]}.$$

The corresponding output current may be written as

$$I = \frac{S\Delta T}{R + R_L}$$

$$= \frac{Q_0}{\Pi} \cdot \frac{R_\pi}{R_\pi + R + R_L} R_e \left[\frac{\exp j\omega t}{1 + j\omega\tau} \right]$$

where $R_\pi = \Pi S(K + K_L)^{-1}$, and Q/Π is a current source as shown in Fig. 3. The frequency dependence can be accounted for by the capacitance C also shown in Fig. 3, and it may be verified that the time constant is given by

$$\tau = \frac{R_\pi(R + R_L)C}{R_\pi + R + R_L} = \frac{\Pi SC}{K_\pi + K + K_L} .$$

Thus, the electrical equivalent of the thermal capacitance C_H, for a given device time constant, is $C = C_H(\Pi S)^{-1}$ [farads]. Since we may encounter resistance levels of hundredths of an ohm coexisting with time constants of hundreds of seconds, it will be commonplace to have values of 10^4 farads for the equivalent capacitance C.

Using the figure of merit $Z = S^2(RK)^{-1}$, and the Kelvin relation $\Pi = ST$, we can write the Peltier conductance K_π and the resistance R_π as, respectively,
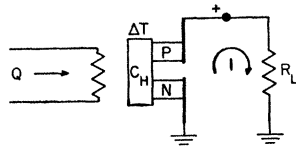
$$K_\pi = \frac{R}{R + R_L} \cdot ZT \cdot K$$

Fig. 1—Schematic of thermoelectric converter, emphasizing the thermal capacitance C_H at the hot junctions. The device also has the internal parameters, K the thermal conductance, R the electrical resistance, as well as the Seebeck and Peltier coefficients S and Π, respectively.
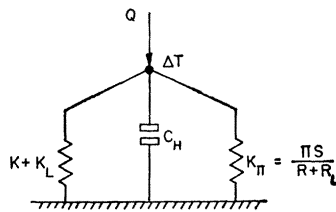

Fig. 2—Equivalent thermal circuit of converter, operating from a constant heat source Q. The equivalent conductance K_π represents Peltier heat pumping.
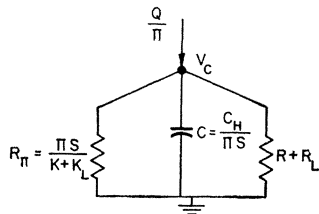

Fig. 3—Equivalent electrical circuit. The resistance R_π results from the constant heat input assumption, represented here by the current source Q/Π. Alternatively, the current source could be replaced by a voltage source $SQ(K + K_L)^{-1}$ in series with R_π.

and

$$R_\pi = \frac{K}{K + K_L} \cdot ZT \cdot R.$$

On the basis that the product ZT may have an upper boundary of the order of unity, K_π and R_π can, at most, be somewhat less than K and R, respectively.

A word of caution regarding efficiency: it must be defined as $\eta = I^2 R_L/Q$, which reduces to

$$\frac{\Delta T}{T} \cdot \frac{R_\pi R_L}{(R_\pi + R + R_L)^2}$$

rather than

$$\frac{R_\pi R_L}{(R_\pi + R + R_L)(R + R_L)}$$

as one might deduce from Fig. 3. Despite low efficiencies, thermoelectric devices may provide a convenient means to simulate long time constants in control problems. The input could be supplied electrically either by Joulean heating or by Peltier pumping, giving rise to quadratic and linear input/output relations, respectively.

E. L. R. Webb
Radio and Electrical Engrg. Div.
Natl. Res. Council
Ottawa, Canada

A Method for Generating Signals of Arbitrary Yet Frequency-Independent Phase Differences*

When testing phase-measuring devices or synthesizing polyphase voltages, or in connection with auto-correlation procedures, function generation, etc., it is often useful to have a source of two or more signals at the same variable frequency, but with continuously adjustable, frequency-independent phase differences. It is the purpose of this note to describe one particularly simple method by which this can be achieved.
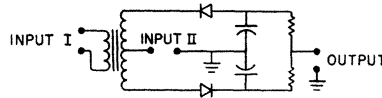

Fig. 1—Balanced-peak detector.

If, in the balanced-peak detector circuit shown in Fig. 1, a sine wave of large amplitude is applied to one of the input terminals and another sine wave of small amplitude and slightly different frequency is applied to the other, the output signal will be a sine wave at the difference frequency with an amplitude corresponding directly to that of the weaker input signal. If the two input signals are expressed as

$$E_1(t) = A_1 \cos(\omega_1 t + \Phi_1) \tag{1}$$

and

$$E_2(t) = A_2 \cos(\omega_2 t + \Phi_2) \tag{2}$$

where

$$A_1 \gg A_2, \tag{3}$$

the output signal will be

$$e_1(t) = A_2 \cos\left[(\omega_1 - \omega_2)t + \Phi_1 - \Phi_2\right]. \tag{4}$$

Here, ω_1 and ω_2 are the angular speeds of the two input signals, A_1 and A_2 are the respective peak amplitudes, and Φ_1 and Φ_2 correspond to some arbitrary phase angles. It is seen that by changing the phase of either one of the input signals, the phase of the output signal will change by the same amount. Consequently, in an arrangement such as is shown in Fig. 2, output signals of independently-adjustable phase differences can be obtained. By adjusting the frequency of the undelayed input signal, the frequency of these output signals can be varied over a wide range without changing their mutual phase relationships.

It should be noticed that it is the stronger of the two input signals that is being phase shifted. This implies that the changes in amplitude commonly associated with varying the phase of a signal will not have any effect on the output.

The actual operation of the arrangement shown in Fig. 2 has been experimentally tested. Two commercially-available signal generators were used as signal sources, and a continuously-variable delay line constituted the phase shifter. The two balanced detectors with the associated low-pass filters were identically constructed so as to cancel the effect of any phase shifts occurring therein. The fixed frequency of the one signal source was arbitrarily chosen to be 100 kc, implying that each microsecond of delay gave a 36° phase shift.

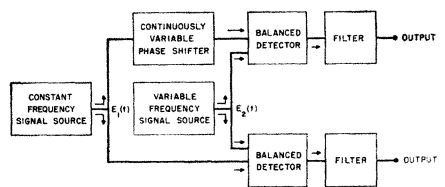The result of the test is illustrated in Fig. 3. As can be seen there, the phase dif-

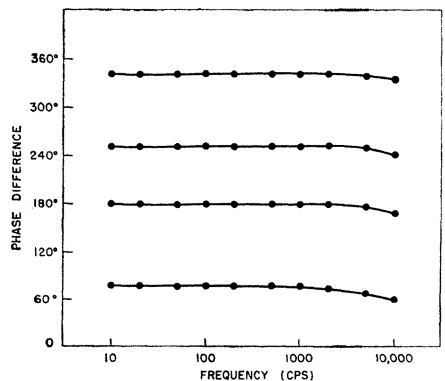Fig. 2—Arrangement for obtaining signals of arbitrary, yet frequency-independent phase differences.

Fig. 3—Performance of the arrangement shown in Fig. 2.

ference between the two output signals at several different phase settings remained constant (within the ±1° inaccuracy of the phase meter) over a range from 10 cps to 1 kc. Above 1 kc, a gradual change in phase was noticed—probably due to nonsymmetrical effects in the detectors and/or filters. No attempts were made to correct this condition. The limitations of the phase meter prevented any phase measurements below 10 cps. However, by observing Lissajous patterns on an oscilloscope, it appeared as if the phase relationship of the output signals remained constant down to essentially dc conditions. This, of course, was to be expected. The minimum operating frequency will be limited by the stability of the signal sources, rather than by the capabilities of the detectors and filters or of the method itself.

The author wishes to thank R. Geitka who constructed the apparatus and performed the testing involved.

O. K. NILSSEN
Sci. Lab.
Ford Motor Co.
Dearborn, Mich.

The Operation of Radio Altimeters Over Snow-Covered Ground or Ice*

The mode of reflection in the ground for the HF signals used in vertical incidence by ionospheric recording at the Royal Society Base at Halley Bay has been studied by Piggott and Barclay.[1] Several types of experiment show that the ice shelf is effectively transparent at HF and that most of the signal is reflected from the sea below the ice shelf rather than from the top of the shelf.

The purpose here is to draw attention to a possible source of danger when using radio altimeters in aircraft which may be particularly important when landing on flat surfaces covered by snow. Owing to a low density of even compacted snow, the signal from the air-snow interface is weak compared with that from the main reflecting interface. The actual circumstances, however, are not too common, and it is, therefore only necessary to give a very crude analysis which indicates the factors involved, and hence the occasions on which special precautions may be desirable.

When a plane wave passes through a dielectric material and is totally reflected at the lower surface of this material, the strength of the signal reflected from the upper surface increases with the dielectric constant of the material, and that from the lower surface decreases with it, the total energy being con-

¹ W. R. Piggott and L. W. Barclay "The reflection of radio waves from an iceshelf," *J. Atmos. and Terres. Phys.*, in press; 1961.

stant. The measurements at Halley Bay show that the partially reflected signal on frequencies near 3 Mc is 17 db weaker than the signal from the sea beneath the iceshelf.

Two factors determine the intensity of a signal reflected from a snow surface:

1) The mean density at the snow in the boundary layer in which reflection occurs, which is about a quarter of a wavelength thick.

2) The rate of change of density with depth, expressed in wavelengths in the medium, which determines whether the boundary should be considered to be sharp or diffuse. The partial reflection coefficient decreases as the boundary becomes more diffuse.

For altimeters operating near 100 Mc, wavelengths of about 3 meters, we may expect the partial reflection to occur within about 1 meter of the top surface.

The average density of snow at this depth is about 0.4 gm/cc so that the partial reflection loss at the air-snow surface is 23db. If the underlying reflector is the sea, the reflection at the top surface for a plane wave will be about 22 db weaker than that from the sea; if the lower reflection is from an iceshelf, the difference will be about 10 db. Frozen ground will lie between these limits. Thus the top surface reflection can be weak relative to that from the lower surface. This can be dangerous when the instrument is such that a weak reflection can be overlooked or is suppressed by a stronger signal reflected from similar ranges.

W. R. PIGGOTT
Dept. of Sci. and Industrial Res.
Radio Res. Station
Ditton Park
Slough, Bucks, England

High-Efficiency Variable-Reactance Frequency Multiplier*

The theory, design and performance of some maximum-efficiency variable-reactance frequency multipliers have been presented by the authors.[1,2] In view of the interest shown at the time of presentation, it is felt that some additional results would be welcomed. In this correspondence, the authors wish to report that a conversion efficiency of 40 per cent was obtained for a fifteen-times passive frequency multiplier

¹ T. Utsunomiya and S. Yuan, "Theory, Design and Performance of Maximum Efficiency Variable Reactance Frequency Multiplier," Electronics Res. Labs., School of Engrg., Columbia University, New York, N. Y., Tech. Rept. No. T-1/164, June 15, 1960.
² T. Utsunomiya and S. Yuan, "Theory, Design and Performance of Maximum Efficiency Variable Reactance Frequency Multiplier," Presented at the Annual Electron Devices Meeting of 1960, Washington, D. C.

using variable-capacitance diodes. Based on the disclosed theory, a quintupler was cascaded with a tripler. The results presented by the authors at the PGED meeting are reproduced here as shown in Fig. 1, where the efficiency vs harmonic number curve is compared with that reported by Leeson and Weinreb[3] and that of the ideal diode. Experimentally measured efficiencies confirmed theoretical estimation closely for harmonic order $N \leq 5$. A theoretical estimation for an eight-times multiplier is also indicated.

① NONLINEAR REACTANCE, PRESENT COLUMBIA UNIV. E.R.L. RESULTS

② NONLINEAR REACTANCE, REPORTED BY LEESON AND WEINREB.
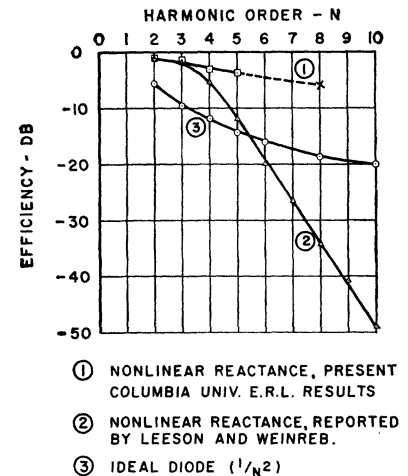
③ IDEAL DIODE $(1/N^2)$

Fig. 1—Efficiency in db vs harmonic number.

In cascading the two multipliers, the following conditions have to be satisfied to assure high efficiency, where efficiency, η, is defined as

$$\eta = \frac{(\text{Output power at } Nf)}{(\text{Total input power})}.$$

1) The voltages across the nonlinear capacitors of both units have to be maximum without causing the diodes to conduct in the forward region.

2) The impedance levels of the two multipliers have to be matched to assure maximum power transfer from one unit to the next.

3) The tripler is used for the output stage because it is more effective in eliminating the undesired harmonics at the output.

The unit tested was operated with an input frequency of 0.84 Mc and an output frequency of 12.6 Mc. The input power to the device was approximately 10 mw, and the output power was 4 mw, which gave the efficiency of 40 per cent.

T. UTSUNOMIYA
The Faculty of Engineering
University of Tokyo
Tokyo, Japan
S. YUAN
Electronics Res. Labs.
School of Engrg.
Columbia University
New York, N. Y.

³ D. B. Leeson and S. Weinreb, "Frequency multiplication with nonlinear capacitors—a circuit analysis," PROC. IRE, vol. 47, pp. 2076–2084; December, 1959.

Parametric Up-Converter Tunable Over an 18:1 Frequency Band*

The operation of parametric amplifiers over frequency bands of an octave or more has not been extensively reported in the literature and indeed these devices have come to be regarded as essentially narrow-band amplifiers with typical frequency bandwidths of 10 per cent to 20 per cent.

Theoretical considerations did not indicate that these restricted bandwidths were necessarily associated with the upper sideband up-converter and an experimental investigation was carried out to explore the bandwidth limitations over wider frequency ranges in a device of this type. Signal frequency was varied over the range 100–1800 Mc and the pump frequency over the range 8500 to 6800 Mc to give a constant upper sideband frequency of 8600 Mc.
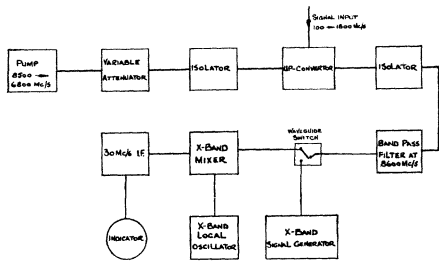

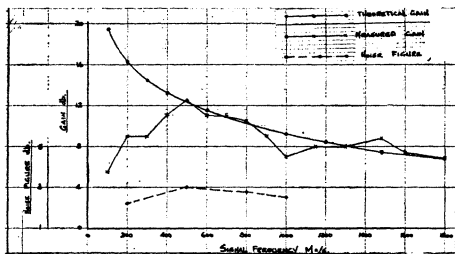Fig. 1—Block diagram of experimental arrangement for up-converter measurements.

Fig. 2—Gain of up-converter.

With the amplifier illustrated in Fig. 1 gain has been obtained over the signal frequency range of 100–1800 Mc by varying only the pump and signal frequencies; no other tuning adjustments to the circuit were necessary. Particular care was taken to utilize an essentially aperiodic signal input circuit. The curves of measured gain and noise figure against frequency are shown in Fig. 2 together with the curve of the theoretical gain based on the Manley-Rowe frequency ratio relationship. It will be noted that the measured gain approaches the theoretical gain over the central and higher portion of the frequency range, while over the lower part of the frequency range the measured gain is lower than the theoretical curve. In the lower frequency region this is due largely to a poor match at the signal input. Thus, over the band 100–1800 Mc the band limits are set by the poor input match at the

* Received by the IRE, January 10, 1961.

lower end and by fundamentally low gain due to the small frequency ratio at the upper end.

The accuracy of the gain measurements, dependent on the absolute calibration of two signal generators operating at the upper sideband and signal frequencies, is estimated to be ±2 db. The noise figure measurements are included as an indication of the approximate noise level which is being investigated further. The pump power required was 250 mw. The diode used was a G.E.C. Type VX3333 with a cutoff frequency of 87 kMc.

Particular care was taken in the design of the amplifier to exclude the pump and the lower sideband signals from the output by means of a band-pass filter which passed only the upper sideband frequency. Ferrite isolators were used in the pump input and signal output waveguides to reduce the effects of unwanted reflections on the fields due to the pump and the two sidebands at the diode. This isolation was important in obtaining the wideband performance of the amplifier.

With the pump adjusted for amplifier gain at a signal frequency of 1000 Mc the rejection by the amplifier of input signals at frequencies which were submultiples of 1000 Mc is shown in Fig. 3. This characteristic is of importance when considering the level of spurious responses associated with the amplifier.
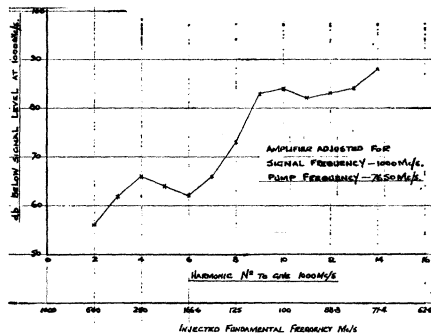

Fig. 3—Harmonic rejection of up-converter.

With the pump at a fixed frequency and the signal frequency varied, the gain was measured to determine the bandwidth over which it was obtained. This bandwidth was, as expected, wide and was found to be in excess of 150 Mc, measurement being restricted only by the tuning characteristics of the particular X-band superheterodyne receiver used as a detection device.

The above results do not necessarily represent the ultimate limits of operation of an upper sideband up-converter over the wide band of signal frequencies. They illustrate only the present state of the development of a wide-band amplifier and are considered to be of sufficient significance and general interest to warrant publication at this interim stage. Investigation of the amplifier characteristics continues.

G. P. SHEPHERD
D. G. KIELY
Royal Naval Scientific Service
Admiralty Surface Weapons Est.
Portsdown, Cosham, Port mouth,
Hants, England

Parametric Amplification by Charge Storage*

When semiconductor diodes are used for parametric amplification, it is usually assumed that it is the variable depletion layer capacitance that provides the amplification. It is the purpose of this letter to point out that parametric amplification and subharmonic oscillation[1] can also be obtained from the effects of charge storage in diodes.[2]

A typical circuit for achieving parametric amplification at relatively low frequencies is shown in Fig. 1(a) and the theory of operation of this circuit in terms of the variable depletion layer capacitance has been extensively studied; however, as will be explained, this circuit can also be shown to provide parametric amplification by charge storage.
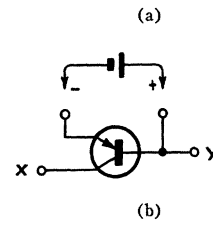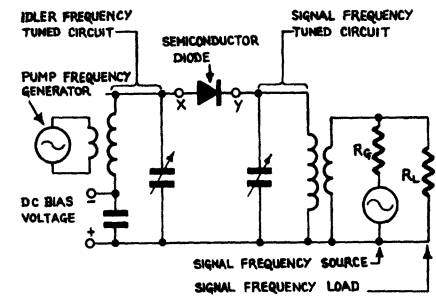

(a)

(b)

Fig. 1.

In studying the effects of charge storage on parametric amplification, transistors have been found useful, since the quantity of charge in the base region can be controlled, to some extent, by the emitter or collector. Now, if in the circuit of Fig. 1(a) we use the base collector junction of a transistor instead of a diode, as indicated by Fig. 1(b), then parametric amplification can be obtained due to the variable depletion layer capacitance. However, if the collector junction is driven into forward conduction during part of the pump cycle, and the pump frequency is not too low, then charge storage will occur; *i.e.*, the charge of minority carriers built up in the base region during forward conduction will allow the junction to continue conducting for part of the time during which the pump voltage reverse biases the diode. This charge storage can be almost completely eliminated by connecting a bat-

tery directly between emitter and base, so as to reverse bias the emitter junction. This has the effect of sweeping nearly all the minority carriers out of the base region within the transit time, so that, provided the pump frequency is not too high, there will be effectively no minority carriers left in the base to provide conduction during reverse bias. The connection of the battery has no effect on the depletion layer capacitance, however.

In all experiments carried out on the circuit of Fig. 1(a) using a transistor as described above, it has been found easy to obtain parametric amplification or subharmonic oscillation, provided the battery is disconnected and the base collector junction is driven into forward conduction. However, if the battery is connected, or the junction not driven into forward conduction, then the amplification or oscillation is greatly reduced, whence it is concluded that charge storage is principally responsible for the parametric effects observed.

In some of the parametric amplifiers that have been reported, the diodes are described as self biased[3] or zero biased,[4] in which cases the diode must be driven into forward conduction during part of the pump cycle; this must also occur if any rectified current is obtained. It thus seems probable that the amplification obtained in many parametric amplifiers depends, at least in part, on charge storage.

D. L. HEDDERLY
British Telecommunications Research Ltd.
Taplow Court, Taplow, Nr. Maidenhead
Berkshire, England

[3] E. M. T. Jones and J. S. Honda, "A low-noise up-converter parametric amplifier," 1959 IRE WESCON CONVENTION RECORD, pt. 1, pp. 99–107.
[4] M. Uenohara, "Noise considerations of the variable capacitance parametric amplifier," PROC. IRE, vol. 48, pp. 169–479; February, 1960.

Approximate Method of Calculating Electromechanical Coupling Factor*

Usually, the electromechanical coupling factor k of the piezoelectric material is calculated from the series resonance frequency f_s and the parallel resonance frequency f_p of the fundamental mode in an appropriate transducer by the following equation (notations following IRE standards on piezoelectric crystals[1] are used unless otherwise mentioned):

$$k^2/(1 - k^2) = (1/p)(f_p^2 - f_s^2)/f_s^2. \quad (1)$$

Or in the first approximation, by putting $\Delta f = f_p - f_s$,

$$k^2 = (2/p)(\Delta f/f_s). \quad (2)$$

Eq. (1), however, is an approximate formula and an error increases with k as shown in Table I. The writer found a better approxi-

TABLE I
CALCULATED VALUES OF k_{31}

Calculated from \ $\Delta f/f_s$	0.1	0.2	0.3	0.5	1.0
Eq. (2)	0.497	0.702	0.860	1.111	1.507
Eq. (19)	0.474	0.641	0.755	0.907	1.110
Eq. (1)	0.454	0.593	0.678	0.779	0.887
Eq. (18)	0.463	0.614	0.710	0.828	0.962
Exact Eq. (21)	0.464	0.616	0.714	0.838	1.000

mate formula (18). This is simpler than (1), and an error may be neglected even when k reaches 0.7.

When the electric equivalent circuit of the vibrator is considered,

$$C_1/C_0 = 1/r = (f_p^2 - f_s^2)/f_s^2, \quad (3)$$

where C_0 is the shunt capacitance and C_1 is the motional capacitance in the fundamental mode. Generally, $C_0 \approx C^{Cl}$, where C^{Cl} is the "clamped" capacitance, and the factor $\chi(\approx 1)$ is introduced[1] which takes into account the influence of the other modes of the vibrator excitable with the same electrode arrangement.

$$C^{Cl}/C_0 = \chi. \quad (4)$$

For the specimen with a single series of modes as fulfilled, e.g., for the length-extensional mode of a bar, the contour-shear mode of a square plate, and the radial mode of a disk, the general electric equivalent circuit, which is correct in all the frequency range, is represented by connecting, in parallel, C^{Cl} (C_1 and L_1 in series), (C_2 and L_2 in series), $\cdots$ (C_∞ and L_∞ in series), the resistance terms being neglected. Namely, the admittance Y of the specimen is as follows:

$$Y = j\omega C^{Cl} + \sum_{n=1}^{\infty} \frac{j\omega C_n}{1 - \omega^2 L_n C_n}. \quad (5)$$

That (5) is an exact solution is proved as follows: generally, Y is solved rigorously from the theory of vibrations as

$$Y = j\omega C^{Cl} \left\{ 1 + \frac{k^2}{1 - k^2} \frac{1}{f(\omega)} \right\}, \quad (6)$$

and

$$f(\omega_{Rn}) = 0, \quad (n = 1, 2, 3, \cdots); \quad (7)$$

where ω_{Rn} is the resonance angular frequency of the nth overtone mode. By Mittag-Leffler's theorem,[2] $1/f(\omega)$ is developed as

$$\frac{1}{f(\omega)} = \sum_{n=1}^{\infty} \frac{p_n}{1 - (\omega^2/\omega_{Rn}^2)}, \quad (8)$$

where p_n is a constant, and especially

$$p_1 = p. \quad (9)$$

Substituting (8) in (6), we obtain

$$C_n = p_n \frac{k^2}{1 - k^2} C^{Cl}, \quad (10)$$

$$L_n = 1/(\omega_{Rn}^2 C_n). \quad (11)$$

[2] E. T. Whittaker and G. N. Watson, "Modern Analysis," Cambridge University Press, Cambridge, Eng., pp. 134–136; 1935.

Now, at the frequency near the resonance of the fundamental mode,

$$\omega^2 L_n C_n \ll 1 \quad (n = 2, 3, 4, \cdots), \quad (12)$$

and we can approximate as

$$C_0 = C^{Cl} + \sum_{n=2}^{\infty} C_n$$
$$= C^F - C_1, \quad (13)$$

where C^F is the "free" capacitance, namely

$$C^F = C^{Cl} + \sum_{n=1}^{\infty} C_n$$
$$= C^{Cl}/(1 - k^2). \quad (14)$$

From (13), (14), (10) and (9), we obtain

$$C_0/C^{Cl} = (1 - pk^2)/(1 - k^2) \quad (15)$$

$$C_1/C^{Cl} = pk^2/(1 - k^2). \quad (16)$$

Accordingly, by comparing (15) and (16) with (3), we obtain

$$k^2 = \frac{1}{p(1 + r)}, \quad (17)$$

or

$$k^2 = (1/p)(f_p^2 - f_s^2)/f_p^2. \quad (18)$$

And when $(\Delta f/f_p)^2$ is neglected,

$$k^2 = (2/p)\Delta f/f_p. \quad (19)$$

Eq. (18) is a new approximate formula, and this approximation is, from (15) and (4), equivalent to

$$\chi = (1 - k^2)/(1 - pk^2), \quad (20)$$

while (1) corresponds to $\chi = 1$.

In Table I, the calculated values by (1), (2), (18) and (19) are compared with true values calculated by (21),[3] in the case of the length-extensional mode where $p = 8/\pi^2$.

$$\frac{\pi}{2}\left(\frac{f_p}{f_s}\right) \tan\left\{\frac{\pi}{2}\left(\frac{f_p}{f_s} - 1\right)\right\}$$
$$= \frac{k_{31}^2}{1 - k_{31}^2}. \quad (21)$$

M. MARUTAKE
Kobayasi Inst. of Phys. Res.
Tokyo, Japan

[3] W. P. Mason, "Piezoelectric Crystals and their Application to Ultrasonics," D. Van Nostrand Co., Inc., New York, N. Y., pp. 61–68; 1950.

A Simple Method of Generating Nanosecond Pulses at X Band*

Present methods of generating nanosecond RF pulses use high-speed switches to amplitude modulate microwave energy. One approach uses fast semiconductor diodes,[1,2] while Beck's[3] utilizes the TWT as a switch. A TWT can also be used in a nonlinear feedback loop to form a regenerative pulse generator.[4] The technique to be described, based on the impulse response of a TWT, is a simple means of generating short RF pulses.

Theoretically, the Fourier spectrum of dc pulses extends out to infinite frequency. For pulses of the order of 1 nsec in width and a few volts amplitude, the components in the X-band region are well above thermal noise at the input of a 50-Ω system. When such short pulses are fed directly into an X-band TWT serving as a band-pass amplifier, RF output pulses comparable in width to the dc input pulses are obtained.

The equipment is shown in Fig. 1; the TWT amplifier consisting of two tubes in cascade gave an estimated 0.5-watt peak-pulse power. The dc pulser produced pulses of 1-nsec base width, rise time of 0.25 nsec and a PRR of 720 pps. The sampling oscilloscope (rise time 0.6 nsec) displays this pulse as shown in Fig. 2(a) and the detected output of the TWT as shown in Fig. 2(b). RF power at the crystal detector (IN23B) was kept low, resulting in square-law operation and a displayed pulse proportional to power. Detected pulse-rise time is about 1 nsec and base pulse width, 2 nsec. Observations on a 2000-Mc traveling-wave oscilloscope gave a rise time of 0.6 nsec and a base pulse width of 1.5 nsec.
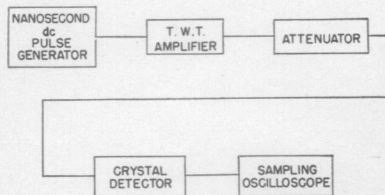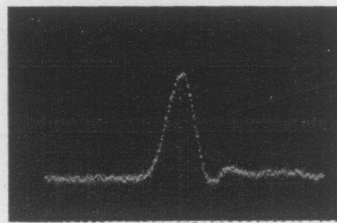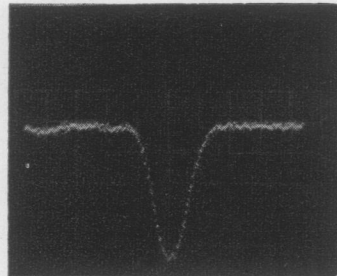

Fig. 1—RF pulse generator using a dc-pulse generator and TWT amplifier.

To study the use of the method in radar applications, the system of Fig. 1 was altered to include transmitting and receiving antennas. Echoes from various objects in the room were observed. Fig. 3(a) shows echoes from two plane metal surfaces 12 feet apart in range, the nearest being 15 feet from the two horn antennas. In Fig. 3(b) the surfaces are about 17 inches apart, the nearest being 40 feet from the antennas. Pulse amplitudes shown are not significant as the reflectors were positioned to give a display convenient

* Received by the IRE, January 23, 1961.
[1] K. J. S. Cave, W. Neu, and A. C. Sim, "A diode modulator for millimetre waves," *Proc. IEE*, vol. 106, pt. B, suppl. No. 16, pp. 759–761; May, 1959.
[2] C. A. Burrus, "Millimicrosecond pulses in the millimetre wave region," *Rev. Sci. Instr.*, vol. 28, pp. 1062–1065; December, 1957.
[3] A. C. Beck, "Waveguide investigation with millimicrosecond pulses," *Bell Sys. Tech. J.*, vol. 35, pp. 35–65; January, 1956.
[4] C. C. Cutler, "The regenerative pulse generator," *Proc. IRE*, vol. 43, pp. 140–148; February, 1955.
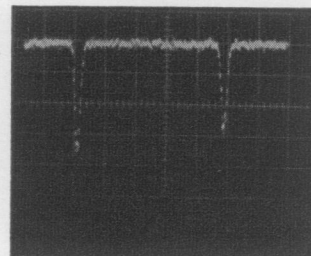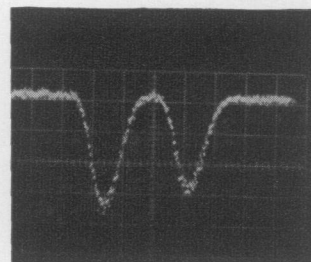
(a)

(b)

Fig. 2—(a) dc input pulse to TWT as observed on a 0.6 nsec rise time sampling oscilloscope. (b) Detected RF output pulse viewed on the same oscilloscope. Horizontal scale is 1 nsec per major division.

(a)

(b)

Fig. 3—(a) Radar echoes from plane metal surfaces 12 feet apart in range and in line with the transmitting and receiving antennas (scale = 5 nsec/major divison). (b) Echoes from plane metal surfaces 17 inches apart (scale = 1 nsec/major division).

for observation. Echoes from plane metal surfaces differing in range by six inches could be resolved easily.

Because the traveling-wave tube is used as an amplifier, this technique is advantageous in setting up a sensitive short-pulse radar. A reflex scheme (Fig. 4) suggested by W. L. Haney uses the same TWT to amplify the received signal. Little additional equipment is required, and the system remains simple. With the setup of Fig. 4, the total gain of the system could not be used, as strong echoes from large objects in the laboratory caused oscillation. Even so, the sensitivity was improved about 25 db.
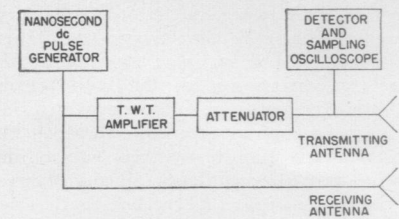

Fig. 4—Sensitive, short-pulse reflex radar.

An application of this method has been independently developed in this laboratory by S. G. Jones and T. H. Shepertycki for obtaining the impulse response of S-band radar receivers. Other applications contemplated for investigation include the location of troublesome reflections on antenna ranges and in "anechoic" rooms. Radar cross-section measurements of small objects and propagation delay studies are also possible.

J. K. PULFER
B. G. WHITFORD
Radio and Elec. Engrg. Div.
Natl. Res. Council
Ottawa, Canada

Whistlers Excited by Sound Waves*

Recently Lippmann[1] has mentioned the possibility that electromagnetic radiation in the low-frequency ranges as produced by a nuclear explosion could propagate as a "Whistler" along the magnetic field of the earth. Lippmann discusses the excitation of this whistler (see under No. 3). We are able to contribute to this discussion considerations which we have made under a more general aspect.[2]

The waves produced directly by the explosion must essentially be of longitudinal character, *i.e.*, they are sound waves. The whistler mode, however, corresponds to waves with essentially transversal polarization. Now Piddington[3] has shown that in the ionospheric plasma four types of electromagnetic waves with different characteristic polarizations can exist; two of them are essentially transversal and the other two essentially longitudinal in polarization. This is due to the influence of the magnetic field of the earth. Both transversal polarizations rotate in an opposite sense. In one sense of polarization, the electric vector rotates in the same way as do the positive ions in their free spiralling movement with the earth's magnetic field as axis; the other sense of polarization corresponds to the free spiral-

* Received by the IRE, January 25, 1961. This work was done under contract No. DA-91-591-EUC-1504 of the U. S. Army.
[1] B. A. Lippmann, "Bomb-excited whistler," *Proc. IRE*, vol. 48, pp. 1778–1779; October, 1960.
[2] K. Rawer and K. Suchy, "Longitudinal- und Transversal-Wellen im Lorentz-Plasma," *Ann. Physik*, vol. 3, pp. 155–170; March, 1959.
[3] J. H. Piddington, "The four possible waves in a magneto-ionic medium," *Phil. Mag.*, vol. 46, pp. 1037–1050; October, 1955.

ling movement of the electrons. In literature these polarizations are mostly designated as "ordinary" and "extraordinary" polarization; following Larenz[1] we prefer to call them "ionic" and "electronic," respectively. The two longitudinal polarizations have also a direct relation with the plasma components; they correspond to a kind of sound wave propagated in the ionic and electronic gas, respectively.

For wave frequencies which are considerably higher than the gyrofrequency of the ions, we can neglect the ionic sound wave. We have recently investigated the relations between the remaining three characteristic waves.[2] The following conclusions regarding the excitation of whistlers by sound waves in a plasma can be obtained:

In the inner ionosphere (below about 300 km), the plasma density increases nearly monotonically with height. This change causes a corresponding continuous change of the characteristic polarizations. The transversal waves which are of purely transversal polarization at the lower border of the ionosphere get a longitudinal component which increases more and more; as to the electronic sound wave which is purely longitudinal at the lower border of the ionosphere we find in the plasma a transversal component increasing more and more. Depending on wave frequency and magnetic field we may find a certain electron density for which the electronic sound wave and the electronic transversal wave have exactly the same polarization. These are the special conditions where an electronic sound wave can excite a transversal wave so that part of the sound wave energy coming from the explosion can be transformed into transversal electromagnetic wave energy.

Fig. 1 is reproduced from our quoted work;[2] it shows the square (w) of the refractive index as a function of the reduced plasma density $X = \omega_N{}^2/\omega^2$ (ω_N plasma pulsation, ω pulsation of the wave). The different curves are valid for the three different characteristic waves in the two limiting cases, i.e., the transversal case ($\theta = \pi/2$) and the longitudinal case ($\theta = 0$). In the latter case, the electronic sound wave reacts with the electronic transversal wave in the transition point which is found on Fig. 1 near $X = 1$. We have shown in the quoted work that in the case of frequencies below the electronic gyrofrequency (for which case Fig. 1 is valid), the transition can only become important when the direction of propagation nearly equals that of the magnetic field. This latter condition is valid in the case of whistlers and our discussion shows that the transition will occur essentially in the neighborhood of that electron density for which the plasma frequency equals the wave frequency.

Another result concerning the absorption of the electronic sound wave can be obtained from our quoted work.[2] This absorption becomes stronger and stronger with increasing angle θ between the direction of wave propagation and that of the magnetic field. As compared with the absorption coefficient of
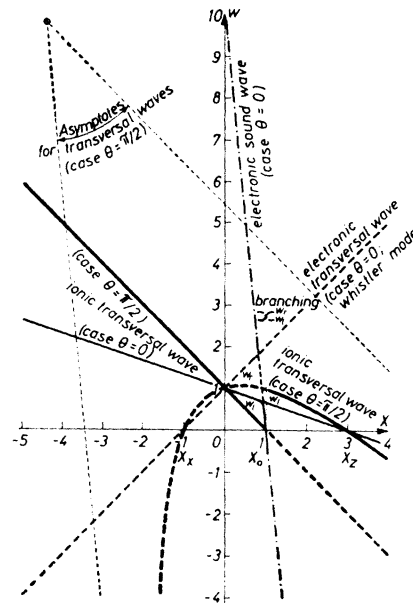

Fig. 1—Effective dielectric factor w ($\approx$square of the refractive index) as a function of the reduced electron density X ($=\omega_N{}^2/\omega^2$) for wave frequency $\omega/2\pi$ =half of the electron gyrofrequency and $3m_e c_0{}^2/(5kT) = 10$. Full lines $=w_l$ =ionic transversal wave, broken lines $=w_r$ =electronic transversal wave, point-dotted lines =electronic sound wave, heavy lines =transversal case ($\theta = \pi/2$), and thin lines =longitudinal case ($\theta = 0$).

the transversal waves, that of the electronic sound wave is greater by about a factor of $3m_e c_0{}^2/(5kT) = 3.556 \cdot 10^9 {}^{\circ}\mathrm{K}/T$. The absorption is very large so that only very strong sound waves are able to produce observable transversal electromagnetic waves. It seems quite reasonable that nuclear explosions at great altitude excite such strong sound waves.

K. RAWER
Ionosphären-Institut
Breisach/Rh., Germany
K. SUCHY
Abtl. theoretische Physik
Physikalisches Institut
der Universität
Marburg/Lahn, Germany

Power Carried by the Cyclotron Waves and the Synchronous Waves on a Filamentary Electron Beam*

Waves on a filamentary electron beam in a transverse-field slow-wave circuit have been analyzed by A. E. Siegman,[1] who found the existence of the fast and slow cyclotron waves, as well as fast and slow synchronous waves, on such an electron beam. It is the purpose of this paper to show that the same result can be expressed in a different way by introducing the concept of the effective

transverse current K and "the synchronous voltage," S, as well as "Chu's kinetic voltage," U. It is found that quite similar expressions for the beam admittance and the power of each wave component to those of the longitudinal electron beam can be obtained by this analysis.

The following equations are obtained from the force equation for electrons which are travelling to the z direction with velocity u_0 under dc conditions in an axial magnetic field B_0.

$$\frac{dU_-}{dt} - j\omega_c U_- = u_0 E_-$$

$$\frac{dU_+}{dt} + j\omega_c U_+ = u_0 E_+ \tag{1}$$

$$\frac{d}{dt}(U_- + jB_0 u_0 r_-) = u_0 E_-$$

$$\frac{d}{dt}(U_+ - jB_0 u_0 r_+) = u_0 E_+ \tag{2}$$

where the definitions of quantities are given as follows:

$U_\pm$ = Chu's kinetic voltage, $-(m/e)\, u_0 v_\pm$

$v_\pm$ = transverse velocity of the electrons in the beam

ω_c = cyclotron angular frequency

$r_\pm$ = transverse displacement of the electron beam

$E_\pm$ = transverse electric field applied to the electron beam

A_+ = positive circularly-polarized component of quantity A

A_- = negative circularly-polarized component of quantity A.

Now, we define a new parameter S which is named "synchronous voltage" because of the effective voltage for the synchronous waves (the author does not believe, however, that this name is the most suitable one).

$$S_- = U_- + jB_0 u_0 r_-$$

$$S_+ = U_+ - jB_0 u_0 r_+. \tag{3}$$

Eq. (2) can be rewritten by the definition in (3) as follows:

$$\frac{d}{dt}S_- = u_0 E_-$$

$$\frac{d}{dt}S_+ = u_0 E_+. \tag{4}$$

The effective transverse current K caused by the displacement of the electron beam from dc value is given as follows:[2]

$$K_\pm = j\omega\sigma_0 r_\pm, \tag{5}$$

where σ_0 is the total charge of the electron beam per transverse unit area. From (3) and (5) the following relationships are obtained:

$$K_- = -\frac{\omega}{\omega_c}\frac{|I_0|}{2V_0}(S_- - U_-)$$

$$K_+ = \frac{\omega}{\omega_c}\frac{|I_0|}{2V_0}(S_+ - U_+), \tag{6}$$

where V_0 is the dc accelerating voltage corresponding to the drift velocity u_0, and I_0 is the dc beam current ($|I_0| = -\sigma_0 u_0$).

[1] A. E. Siegman, "Waves on a filamentary electron beam in a transverse-field slow-wave circuit," *J. Appl. Phys.* vol. 31, pp. 17–26; January, 1960.

[1] K. W. Larenz, "Beitrag zur Magneto-Hydrodynamik kompressibler Medien," presented at lecture in Bad Salzuflen, Germany; April, 1952 (unpublished).

[2] H. A. Haus, "Electron Beam Waves in Microwave Tubes," in "Electronic Wave Guides," Polytechnic Press, New York, N. Y.; 1958.

The effective voltage and current for the cyclotron waves themselves can be obtained by putting $E_\pm = 0$ and $S_\pm = 0$ in (1) and (6) as follows:

$$U_- = U_{f-}e^{-j(\beta_e+\beta_c)z} \cdot e^{j\omega t}$$

$$U_+ = U_{s+}e^{-j(\beta_e-\beta_c)z} \cdot e^{j\omega t} \qquad (7)$$

$$K_- = \frac{\omega}{\omega_c} \frac{|I_0|}{2V_0} U_{f-}e^{-j(\beta_e+\beta_c)z} \cdot e^{j\omega t}$$

$$K_+ = -\frac{\omega}{\omega_c} \frac{|I_0|}{2V_0} U_{s+}e^{-j(\beta_e-\beta_c)z} \cdot e^{j\omega t}, \qquad (8)$$

where $\beta_e = \omega/u_0$, $\beta_c = \omega_c/u_0$. The power carried by the fast and slow cyclotron waves can be given by the generalized Chu's power theorem as follows:

$$P_f = \tfrac{1}{2} \operatorname{Re}[U_-K_-{}^*] = \frac{|I_0|}{4V_0} \frac{\omega}{\omega_c} |U_{f-}|^2$$

$$P_s = \tfrac{1}{2} \operatorname{Re}[U_+K_+{}^*] = -\frac{|I_0|}{4V_0} \frac{\omega}{\omega_c} |U_{s+}|^2. \qquad (9)$$

The characteristic beam admittance for the small-signal quantities of the cyclotron waves is expressed by (7) and (8) as follows:

$$Y_0 = \frac{K_-}{U_-} = -\frac{K_+}{U_+} = \frac{\omega}{\omega_c} \frac{|I_0|}{2V_0}. \qquad (10)$$

This expression is very similar to that for the longitudinal beam (one-dimensional) given by the following equation.

$$Y_0 = \frac{\omega}{\omega_q} \frac{|I_0|}{2V_0}, \qquad (11)$$

where ω_q is the reduced plasma angular frequency.

The same equations as (7) and (8) for the synchronous waves can be obtained by putting $E_\pm = 0$ and $U_\pm = 0$ in (4) and (6):

$$S_- = S_{s-}e^{-j\beta_e z} \cdot e^{j\omega t}$$

$$S_+ = S_{f+}e^{-j\beta_e z} \cdot e^{j\omega t} \qquad (12)$$

$$K_- = -\frac{\omega}{\omega_c} \frac{|I_0|}{2V_0} S_{s-}e^{-j\beta_e z} \cdot e^{j\omega t}$$

$$K_+ = \frac{\omega}{\omega_c} \frac{|I_0|}{2V_0} S_{f+}e^{-j\beta_e z} \cdot e^{j\omega t}. \qquad (13)$$

Also, the power carried by the slow and fast synchronous waves are

$$P_s = \tfrac{1}{2} \operatorname{Re}[S_-K_-{}^*] = -\frac{|I_0|}{4V_0} \frac{\omega}{\omega_c} |S_{s-}|^2$$

$$P_f = \tfrac{1}{2} \operatorname{Re}[S_+K_+{}^*] = \frac{|I_0|}{4V_0} \frac{\omega}{\omega_c} |S_{f+}|^2. \qquad (14)$$

The characteristic beam admittance is given as (10).

It should be noticed that the power given by (9) and (14) is not the true transverse power (meaning, strictly speaking, the energy transfer due to the transverse fields), but the total power carried by each wave as pointed out by Siegman. This is because the effective transverse current K given by (5) is not the true transverse displacement current which should be

$$K_{\pm\text{true}} = \left(j\omega + u_0\frac{\partial}{\partial z}\right) r_\pm \sigma_0 = v_\pm \sigma_0. \qquad (15)$$

And so,

$$K_{\pm\text{true}} = \frac{|I_0|}{2V_0} U_\pm \text{ for the cyclotron waves}$$

$$K_{\pm\text{true}} = 0 \text{ for the synchronous waves.} \qquad (16)$$

Therefore, the true power in the transverse direction, P_t, is

$$P_{t\text{ cyc}} = \tfrac{1}{2} \operatorname{Re}[U_\pm K_\pm{}^*{}_{\text{true}}] = \frac{|I_0|}{4V_0} |U_\pm|^2.$$

$$P_{t\text{ syn}} = 0 \qquad (17)$$

P_ts for the fast and slow cyclotron waves are both positive and the same because of the kinetic power due to the cyclotron rotation of electrons in the transverse direction. P_ts for the synchronous waves are zero because there is no transverse motion of electrons for these waves.

The power in the longitudinal direction can be obtained by substracting P_t from the total power as follows:

$$P_{lf\text{ cyc}} = \left(\frac{\omega}{\omega_c} - 1\right)\frac{|I_0|}{4V_0} |U_{f-}|^2$$

$$P_{ls\text{ cyc}} = -\left(\frac{\omega}{\omega_c} + 1\right)\frac{|I_0|}{4V_0} |U_{s+}|^2$$

$$P_{lf\text{ syn}} = \frac{\omega}{\omega_c} \frac{|I_0|}{4V_0} |S_{f+}|^2$$

$$P_{ls\text{ syn}} = -\frac{\omega}{\omega_c} \frac{|I_0|}{4V_0} |S_{s-}|^2. \qquad (18)$$

In conclusion, the total power flow along the electron beam discussed here is given as

$$P = \tfrac{1}{2}Y_0[|U_{f-}|^2 - |U_{s+}|^2 + |S_{f+}|^2 - |S_{s-}|^2]. \qquad (19)$$

SHIGEBUMI SAITO
Inst. of Industrial Sci.
University of Tokyo
Tokyo, Japan

Parametric Variable-Capacitor Motor*

The problem of rotary motion with stimulance injected parametrically via a magnetic field has already been solved.[1] An active element appears in the electromagnetic network thanks to the total derivative of $d(Li)/dt$, but a transistor amplifier was included for stimulance enhancement. The underlying integro-differential equation with a Mathieu-Hill-type solution, covering the total electromagnetic system, is of the form

$$L\frac{di}{dt} + \left(R_P + \frac{dL}{dt}\right)i + S\int i\,dt = e(t). \qquad (1)$$

Two operators pertaining to spinning sinors can be identified, inviting the use of the Candy-Hollingworth operational equation solution with hyper-complex numbers, developed in England.[2] One operator is $d/dt \equiv j\omega = j2\pi f = j2\pi 60$ for the driving voltage, and the other is $d/dt \equiv j\Omega = j2\pi n_s$, where n_s is the rotational speed of the motor shaft in turns per second. R_P designates the positive

or loss resistance of the total electromechanical system. It is now very logical to ask the following question: Would the dual of the network covered by (1) possibly yield an additional realizable physical system? If so, we can make a parametric electric motor based on the total differential of $d(Cv)/dt$, where $C = 1/S$ is the variable capacitance. Such a motor would have much in common with the now popular semiconductor diode, variable capacitance, parametric microwave and wide-band amplifier. Replacing magnetic-field injected stimulance by electric-field injected stimulance, we obtain

$$C\frac{dv}{dt} + \left(G_P + \frac{dC}{dt}\right)v + \Gamma\int v\,dt = i(t), \qquad (2)$$

where $\Gamma = 1/L$ is the reciprocal inductance and G_P the positive or loss conductance of the total electromechanical system. With reference to both (1) and (2), transistor amplification may be added for enhanced stimulance, resulting in both cases in a practical brushless electric motor. Both (1) and (2) are linear equations, and rotation may therefore be predicted by the Nyquist stability theorem. It goes without saying that pendulum motion is equally well predicted, and that maintained pendulums may be built this way, provided the proper restoring force is introduced to change the rotary motion into oscillatory motion.[3]

Guided by theoretical speculations of the above nature, the writer carried out experiments with the Class-C amplifier shown in Fig. 1. While the explanation for the opera-
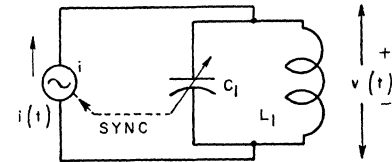

Fig. 1—Basic scheme of making the tuning capacitor in a tank circuit spin around so as to become an electric motor.

tion is given by the term dC/dt in (2), a more direct visualization of how the active element is introduced is obtained from the following reasoning. Let us assume that the moving vanes of the capacitor C_1 in Fig. 1 are on their way into the system of fixed vanes, and that the condition of resonance is approached. Accordingly, the alternating voltage across the capacitor C_1 experiences an increased amplitude, with an electric field attraction force appearing, which aids the movement of the vanes and thus provides a rotational force. All that is needed for practical motor operation is suitable programming of the source $i(t)$, so that self-commutation obtains. The necessary synchronization is indicated by the dotted arrow marked "SYNC" in Fig. 1. To test this idea, the writer removed the stops from the variable capacitor, reduced the friction in the bearings, and with an elementary form of synchronization, the rotor of the variable capacitor began to turn around; the variable capacitor was now an electric motor.[4] Several

different schemes for synchronization were used, all but one of them free from mechanical switching. Thus, the source $i(t)$ in Fig. 1 may represent a tiny high-voltage battery (for example, a 600-volt battery), with the programming device consisting of an electronic switch, controlled capacitively, or otherwise, by the rotating vanes. For a slowly rotating motor, operated at 600 volts, the current drain is less than 1 μa, and the required power of the order of 100 μw. Since there are practically no ri^2-losses, the motor has high efficiency. The simplest programming system is obtained when vdC/dt yields a double-valued force function, sufficient all by itself to accomplish rotation.

Just as a conventional electric motor operates from a lead-cell storage battery, this new motor operates from a capacitor battery (the old Leyden jar battery). The experimental motor runs for several minutes from a 6-μf capacitor, initially charged to 800 volts. This type of motor can be made to produce considerable torque, however, since the air-space capacitance per unit volume can be given a high value and since air dielectric is only a first consideration. For space vehicles, a motor for high voltage and low current may fit available atomic and radiation sources better than conventional motors. If energy storage is not required, the motor may be ac-operated. The freedom from brushes should make this type of lightweight motor reliable and maintenance-free.

<div align="right">

HARRY E. STOCKMAN
Lowell Tech. Inst.
Lowell, Mass.

</div>

The Doppler Effect and Inertial Systems*

If an artificial satellite S transmits a radio signal of frequency $f \gg f_c$, where f_c is the maximum plasma frequency of the ionosphere, an observer P on the earth records a frequency f'. Due to changes of the radial velocity between S and P, the received frequency f' varies in time as illustrated by the Doppler-shift curve of Fig. 1. For linear orbits of S and P, the time derivative of the Doppler-shift curve is described by the identity

$$\lambda(\dot{f}') = -\frac{v_{\text{rel}}^2}{R}\sin^2\psi, \tag{1}$$

where $\lambda = c/f$ is the wavelength of the emitted signal in free space, v_{rel} is the relative velocity between S and P, R is the range, and $\psi = \measuredangle v_{\text{rel}}$, R. From (1) follows the minimum-range equation[1] ($\psi = \pi/2$, $R = R_m$)

$$\lambda(\dot{f}')_{\max} = -\frac{v_{\text{rel}}^2}{R_m}, \tag{2}$$

where $(\dot{f}')_{\max} = tg\alpha_{\max}$. Fig. 1 is the maximum rate of change of the observed Doppler

* Received by the IRE, January 30, 1961.
[1] W. Priester and G. Hergenhahn, "Bahnbestimmung von Erdsatelliten aus Doppler-Effekt Messungen," Westdeutscher Verlag, Köln und Opladen, West Germany; 1958. See especially p. 11.

frequency shift and R_m is the minimum range. With (2) one can evaluate R_m from the measurement of $(\dot{f}')_{\max}$ and from the knowledge of λ and v_{rel}. Eqs. (1) and (2) represent identities which are valid for linear orbits of S and P.

For circular orbits of S, with an observer P assumed at rest relative to this orbit, the minimum-range equation has been previously derived.[2] For the general case of curved orbits of S and P (Fig. 2), one obtains the minimum-range equation

$$\lambda(\dot{f}')_{f'=f} = -\frac{v_{\text{rel}}^2}{R_m} + \frac{v_s^2}{\rho_s}\cos\alpha - \frac{v_p^2}{\rho_p}\cos\beta$$
$$+ \dot{v}_s\cos\gamma - \dot{v}_p\cos\delta, \tag{3}$$

where v_s is the orbital speed of S and ρ_s is the radius of the orbit of S, v_p is the orbital speed of P and ρ_p is the radius of the orbit of P.
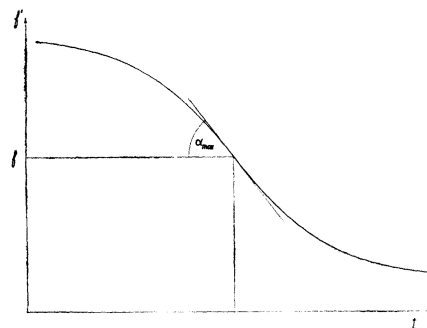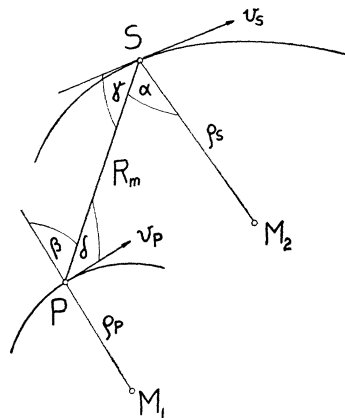

Fig. 1.

Fig. 2.

The second and third term in (3) represent the components of the radial accelerations of S and P in the direction of R_m with the signs corresponding to the angles α, $\beta < \pi/2$ as shown in Fig. 2. The fourth and fifth terms are, respectively, the components of the tangential accelerations of S and P in the direction of R_m for the general case of curved orbits with the signs corresponding to γ, $\theta < \pi/2$. For circular orbits, $\dot{v}_s = \dot{v}_p = 0$. If the orbits of S and P lie in the equatorial plane of the earth and one obtains, e.g., $R_m = 1000$ km from the identity stated in (2), the second term of (3) increases R_m by

[2] K. Toman, "The minimum-range equation and the maximum Doppler-frequency shift for satellites," PROC. IRE (Correspondence), vol. 48, pp. 1339–1340; July, 1960.

15 per cent while the third term of (3) reduces R_m by 0.1 per cent.

A comparison of (2) and (3) discloses that for curved orbits the orbital speeds v_s and v_p, although contained in v_{rel} according to the equation $v_{\text{rel}}^2 = v_s^2 + v_p^2 - 2v_sv_p\cos\epsilon$, appear separately in (3). For $\dot{v}_s = \dot{v}_p = 0$ and $\rho_s = \rho_p = \infty$, (3) reduces to (2). Eq. (2) is valid for inertial systems. Those are systems without acceleration. For accelerated systems (curved orbits), the relative velocity v_{rel} describes inadequately the space-time continuum. Therefore, these nonrelativistic considerations illustrate the concepts of uniform and nonuniform relative motion which are known to underlie the special and the general theory of relativity, respectively.

If v_{rel} alone fulfills the identity of a space-time continuum (2), the special theory of relativity applies; the general theory of relativity is necessary, however, if v_s and v_p appear individually in the identity of a space-time continuum (3). Doppler studies of orbiting satellites are principally subject to the general theory because, for the description of the space-time continuum, v_{rel} and the concept of inertial systems as contained in (2) do not suffice. If they do it is only approximative.

<div align="right">

KURT TOMAN
Air Force Cambridge Res. Lab.
Ionospheric Phys. Lab.
Bedford, Mass.

</div>

Envelope Probability as a Function of E/N_0*

It has been known for some years[1] that: 1) the parameter that determines probability of detection of a signal in additive noise is the ratio of signal energy to noise power per unit bandwidth; and 2) the optimum receiver uses a matched filter (or correlator), which generally does not produce a constant-amplitude sine wave at its output. Nevertheless, almost all (if not all) of the published analyses of detection probability emphasize signal-to-noise power ratio, and use as a model a constant-amplitude sine wave in noise at the input to the envelope detector. It is shown below that the probability density of the envelope of the output of a matched filter can easily be derived in terms of the ratio of signal energy to noise power per unit bandwidth. As a consequence, it is recommended that the use of "noise bandwidth," 3-db bandwidth, and 3-db pulse duration be restricted to situations in which they are really necessary.

The desired relationship can easily be derived with an error of 3 db as follows: Rice's[2] equation 3.10–11 for the probability density of the envelope R of a sine wave with constant amplitude P in additive narrow-

* Received by the IRE, February 6, 1961.
[1] J. L. Lawson and G. E. Uhlenbeck, "Threshold Signals," McGraw-Hill Book Co., Inc., New York, N. Y.; 1950.
[2] S. O. Rice, "Mathematical analysis of random noise," Bell Sys. Tech. J., vol. 23, pp. 282–332, July, 1944; vol. 24, pp. 46–156, January, 1945.

band Gaussian noise with zero mean and variance ψ_0 gives:

$$p(R) = \frac{R}{\psi_0} \exp\left[-\frac{R^2 + P^2}{2\psi_0}\right] I_0\left(\frac{RP}{\psi_0}\right). \quad (1)$$

Since papers on matched filters, such as Turin,[3] show that the peak signal-to-noise power ratio at the output of a matched filter is $2E/N_0$, where E is the input signal energy and N_0 is the input noise power per 1-cps band, one might be tempted to set $P^2/2\psi_0$ equal to $2E/N_0$ in (1). A suspicion that this is not correct could be aroused by an analysis of Manasse[4] that shows that envelope detection reduces the "effective E/N_0" by a factor of at least two. Closer reading of the papers on matched filters shows that envelope detection cannot be assumed in the argument leading to the conclusion that the power SNR is $2E/N_0$.

A direct, correct derivation of the desired relation can be obtained from Dugundji,[5] who shows very simply that, when the input to a (linear) filter with a transfer function $G(j2\pi f)$ is any signal $s(t)$ plus Gaussian noise with zero mean and power spectrum $W(f)$, the first probability density of the envelope R of the filter output is given by (1) above with $|z(t)|$ substituted for P, where:

$$z(t) = 2\int_0^\infty S(j2\pi f)G(j2\pi f)\exp[j2\pi ft]df \quad (2)$$

$$S(j2\pi f) = \int_{-\infty}^\infty s(t)\exp[-j2\pi ft]dt \quad (3)$$

$$\psi_0 = \int_{-\infty}^\infty |G(j2\pi f)|^2 W(f)df. \quad (4)$$

For simplicity, assume that the noise at the filter input is also white.[6] Let $W(f) = N_0/2$. The optimum (matched) filter can be defined[3] by:

$$G(j2\pi f) = kS^*(j2\pi f)\exp(-j2\pi ft_0) \quad (5)$$

where k is a real constant and $s(t)$ will produce a maximum filter output at $t = t_0$. Then

$$\psi_0 = \frac{N_0}{2}\int_{-\infty}^\infty |kS^*(j2\pi f)\exp(-j2\pi ft_0)|^2 df$$

$$= \frac{k^2 N_0}{2}\int_{-\infty}^\infty |S(j2\pi f)|^2 df \quad (6)$$

and

$$z(t) = 2k\int_0^\infty |S(j2\pi f)|^2 \exp[j2\pi f(t - t_0)]df. \quad (7)$$

At $t = t_0$,

$$z(t_0) = 2k\int_0^\infty |S(j2\pi f)|^2 df$$

$$= k\int_{-\infty}^\infty |S(j2\pi f)|^2 df \quad (8)$$

and

$$\frac{z(t_0)|^2}{2\psi_0} = \frac{1}{N_0}\int_{-\infty}^\infty |S(j2\pi f)|^2 df = E/N_0. \quad (9)$$

Thus, (1) above can be converted to apply to the general case of a matched filter followed by an envelope detector (which is optimum when the phase of the signal is unknown and has a constant probability density) by substituting E/N_0 for $P^2/2\psi_0$.

It is of course possible to interpret the above as proving that, for any matched-filter, envelope-detector receiver, there is an equivalent "Rice model" in which the signal has a constant power E/T for duration T, the noise power is N_0B, and $BT = 1$. However, note that the definitions of B and T are completely arbitrary except for their product, so B and T need have no physical significance. Although B and T may be used for convenience in describing the receiver filter and the signal, their use is not required in the "Dugundji model," and this model is a more direct analog of the physical system than the "Rice model." Finally, the Dugundji approach shows directly the effects of using an imperfectly-matched filter, whereas the "Rice model" superficially implies that doubling B increases the required signal power by 3 db. Therefore, it is suggested that B and T be used only where their convenience really justifies their likely misuse.

LEE E. DAVIES
Div. of Engrg. Res.
Stanford Res. Inst.
Menlo Park, Calif.

8- and 11-Gc Nanosecond Carrier Pulses Produced by Harmonic Generation*

Oscillograms have been obtained showing carrier pulses of nanosecond duration and for which the RF carrier is phase locked with the envelope. These pulses have been obtained at carrier frequencies of both 8 Gc and 11 Gc and at pulse repetition rates of 10 and 20 Mc. Both a baseband electrical stroboscope[1] and a new band-pass electrical stroboscope were used to obtain these oscillograms.

The RF pulses are generated directly from the harmonics of the envelope frequency present in the sharp step that is found at the end of the recovery transient of a diffused silicon mesa computing diode.[2,3] The diode, a selected FD-100, is mounted across a waveguide and driven at the baseband repetition frequency. Only the harmonics higher in frequency than the cutoff frequency of the waveguide are propagated. In the present case, a 0.400×0.900-inch waveguide (WR-90) with a low-frequency cutoff of 6.56 Gc was used.

This microwave pulse generator circuitry is shown on the schematic of Fig. 1. From

---

the secondary of the double-tuned output transformer, a high-level sine wave and dc from a self-biasing resistor are applied to the diode. The RF by-pass condenser C_1 is also the tuning capacitor for the secondary of the transformer.

In a test setup used to obtain the 8-Gc carrier pulses at a 20-Mc repetition frequency, a waveguide to coaxial transducer connected the microwave pulse generator of Fig. 1 directly to the coaxial input of the baseband electrical stroboscope.[4] Fig. 2(a) shows an oscillogram of this pulse. The horizontal sensitivity of the stroboscope is 5×10^{-10} seconds per large division. Since 4 phase-locked RF cycles are contained in
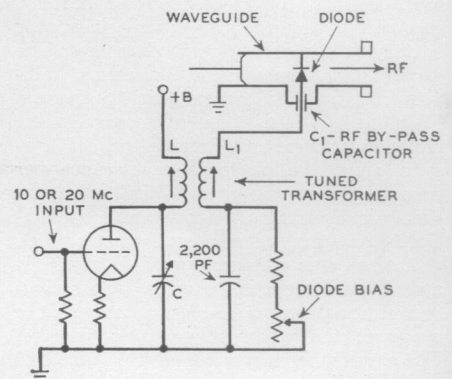

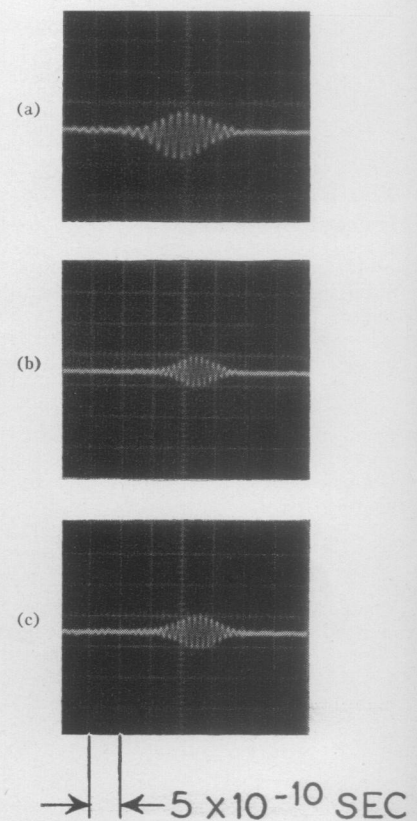Fig. 1—Microwave pulse generator circuitry.

Fig. 2—Oscillograms showing phase-locked carrier cycles within the pulse envelope. (a) 8-Gc pulses at a 20-Mc repetition frequency. (b) 11-Gc pulses at a 10-Mc repetition frequency. (c) 11-Gc pulses at a 20-Mc repetition frequency.

---

[3] G. L. Turin, "An introduction to matched filters," IRE TRANS. ON INFORMATION THEORY, vol. IT-6, pp. 311–329; June, 1960.
[4] R. Manasse, "The Performance of Post-Detection Integrators for the Detection of a Sine Wave in Noise at Low Input Signal-to-Noise Ratio," M.I.T. Lincoln Lab., Lexington, Mass., Group Rept. No. 32-26, ASTIA AD 236 234; November 28, 1956.
[5] J. Dugundji, "Envelopes and pre-envelopes of real waveforms," IRE TRANS. ON INFORMATION THEORY, vol. IT-4, pp. 53–57; March, 1958.
[6] Turin also derives a matched filter for nonwhite input noise.

[1] W. M. Goodall and A. F. Dietrich, "Fractional millimicrosecond electrical stroboscope," PROC. IRE, vol. 48, pp. 1591–1594; September, 1960.
[2] A. F. Boff, J. Moll and R. Shaw, "A new high-speed effect in solid state diodes," Digest of Papers of 1960 Solid States Circuits Conf.; pp. 50–51.
[3] A. F. Dietrich and W. M. Goodall, "Solid-state generator for 2×10^{-10} second pulses," PROC. IRE, vol. 48, pp. 791–792; April, 1960.

[4] Goodall and Dietrich, op. cit.; for block diagram of stroboscope, see Fig. 1, p. 1592.

one division, the time for an individual cycle is 1.25×10^{-10} seconds. This corresponds to a frequency of 8 Gc ($F = 1/T$). The peak pulse power was measured as 0.17 mw.

Fig. 3 shows the block schematic of the band-pass electrical stroboscope used in the test setup to observe the 11-Gc carrier pulses at both a 10- and 20-Mc repetition frequency. The strobe pulse was generated by the same technique as in Fig. 1 but at a 100-cycle lower baseband frequency. This pulse is amplified by a traveling-wave tube which has a 3-db bandwidth of 2 Gc centered at 11.2 Gc. The amplified RF strobe pulse and a similarly amplified RF signal pulse are combined in a 3-db waveguide coupler and demodulated. The detected output, which is a low-frequency replica of the RF signal pulse, was applied to a low-frequency oscilloscope.
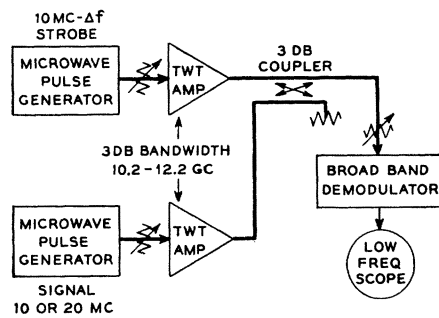
Fig. 3—Block schematic of test setup using band-pass electrical stroboscope.

Fig. 2(b) is an oscillogram of the 11-Gc, 10-Mc repetition-rate pulse with a peak power of 0.004 mw. Fig. 2(c) shows the 20-Mc repetition-rate pulse with a peak power of 0.011 mw. Horizontal sensitivity is the same as Fig. 2(a). In these two oscillograms there are 5.5 phase-locked RF cycles in the 5×10^{-10} seconds period. This corresponds to a frequency of 11 Gc. Using similar techniques, on April 7 oscillograms like Fig. 2 showing 56 Gc pulses at a 160 Mc repetition frequency were obtained.

A. F. DIETRICH
Bell Telephone Labs., Inc.
Red Bank, N. J.

A Variable Dual Reactance Traveling-Wave Parametric Amplifier*

Traveling-wave-type parametric amplifiers have been realized which utilize transmission lines with one reactance being varied by a propagating wave. Tien and Suhl[1] have presented an analysis of parametric amplification in propagating circuits by using one time-varying distributed reactance (inductance) as the coupling element between two propagating media. Similar

results can be achieved by employing two nonlinear distributed reactances (inductance and capacitance) to couple the two transmission lines. The mathematical model presented here, employing two variable distributed coupling reactances, shows that twice as much gain in nepers per unit length of line can be realized over an amplifier where only one coupling reactance is varied. Although the difference frequency between pump and signal is considered, the sum frequency and higher components are neglected, for they may be suppressed in the propagating structure by choosing the proper pump frequency or by designing a propagating structure such that the higher-order sidebands are outside the bandwidth of the circuit.

Thus, we shall consider the nondegenerate case ($\omega_1 \neq \omega_2$) where waves of the signal frequency ω_1 on line No. 1 and waves of the difference or idler frequency ω_2 on line No. 2 are related as follows:

$$\omega_1 + \omega_2 = \omega. \tag{1}$$

These waves are coupled through two distributed reactances which vary in time at the pump frequency ω, and are spatially dependent upon the pump phase shift βz, where

$$\beta = \beta_1 + \beta_2 + \Delta\beta, \tag{2}$$

and z is the longitudinal direction of propagation. That is, the inductive and capacitive coupling reactances between these two lines may vary as follows:

$$L(z, t) = 1/2L[e^{+j(\omega t - \beta z)} + e^{-j(\omega t - \beta z)}],$$

$$C(z, t) = 1/2C[e^{+j(\omega t - \beta z)} + e^{-j(\omega t - \beta z)}],$$

when this coupling network is energized by a traveling-wave of frequency ω and phase constant β. When $\Delta\beta \neq 0$, the system is no longer dispersionless, and it will be shown that the gain of the amplifier is reduced when $\Delta\beta$ deviates from zero. The two pairs of transmission line equations, neglecting series resistance and shunt conductance, are written as

$$\frac{\partial V_1(z, t)}{\partial z} = -L_1 \frac{\partial I_1(z, t)}{\partial t} - \frac{\partial}{\partial t}[L(z, t)I_2(z, t)],$$

$$\frac{\partial I_1(z, t)}{\partial z} = -C_1 \frac{\partial V_1(z, t)}{\partial t} - \frac{\partial}{\partial t}[C(z, t)V_2(z, t)]; \tag{3}$$

$$\frac{\partial V_2(z, t)}{\partial z} = -L_2 \frac{\partial I_2(z, t)}{\partial t} - \frac{\partial}{\partial t}[L(z, t)I_1(z, t)],$$

$$\frac{\partial I_2(z, t)}{\partial z} = -C_2 \frac{\partial V_2(z, t)}{\partial t} - \frac{\partial}{\partial t}[C(z, t)V_1(z, t)], \tag{4}$$

where V and I are, respectively, the voltage and current along a line. These two pairs of simultaneous equations can be readily employed to solve for the gain factor, α, of $I_1(z, t)$. To simplify the equations, let $\eta (\eta \ll 1.0)$ be the ratio of the variable to the fixed reactance whether it be inductive or capacitive, assuming both to vary the same amount for mathematical simplicity. Thus, upon solving (3) and (4) for the gain factor α of the signal current $I_1(z, t)$, we have

$$\alpha = \tfrac{1}{2}(\eta^2\beta_1\beta_2 - \Delta\beta^2)^{1/2} \text{ nepers per unit length.}$$

The corresponding term for a single vari-

able coupling reactance (either inductance or capacitance) traveling-wave parametric amplifier is

$$\alpha = \tfrac{1}{4}(\eta^2\beta_1\beta_2 - 4\Delta\beta^2)^{1/2} \text{ nepers per unit length.}$$

Therefore, the gain in nepers per unit length α is doubled by employing two variable coupling reactances rather than one when $\Delta\beta = 0$, *i.e.*, when the system is dispersionless. This condition exhibits optimum gain. As shown in Fig. 1 with $\Delta\beta \neq 0$, the gain of the variable dual reactance amplifier decreases much less rapidly with increasing dispersion than does the single variable reactance device. Also, the dual amplifier can operate with considerable dispersion before the gain in nepers per unit length drops to a value equal to that of a nondispersive single-reactance amplifier. Thus, the dual device can be made to perform over a much greater gain-dispersion area than the conventional amplifier, provided the amplifier can be made stable. Finally, the dual amplifier would exhibit a better noise figure than the single amplifier if both devices exhibited approximately the same loss per unit length of line (with the pump off), since the dual device possesses more gain.
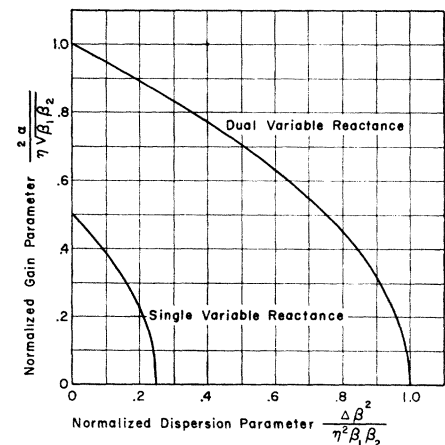

Fig. 1—Normalized gain dispersion characteristics for single and dual variable reactance traveling-wave parametric amplifiers.

This type of distributed parametric amplifier could possibly be realized with two transmission lines, in close proximity, immersed in a continuous medium consisting of both ferroelectric and ferromagnetic material, with the time-varying coupling capacitance and inductance being supplied by the nonlinear characteristics of each material, respectively. However, present-day materials would have to be greatly improved for such an amplifier to operate effectively. The entire structure might then be surrounded by some form of guided wave structure which would transmit the energizing pump wave. It should be noted that the distributed parametric amplifier is a relatively broad-band device and since the gain per unit length is proportional to the product of signal and idler phase constants, broad-band, low loss, slow-wave-propagating structures should be employed for high-gain and low-noise performance.

ROBERT D. WANSELOW
Microwave Tube Div.
Hughes Aircraft Co.
Los Angeles, Calif.

Parametric-Excited Resonator Using Junction Transistor*

In recent correspondence, the subject of the junction transistor as a three-terminal capacitor has been discussed.[1-3] A note by Giacoletto[3] describes an interesting phenomenon—the capacitive interaction between emitter and collector junctions of a transistor in the cutoff state.

The author discovered and utilized this phenomenon independently in early 1959, while working on the parametric-excited resonator using semiconductor junction devices, and reported it in his M.S. thesis (August, 1959), on which this note is based.

Fig. 1 shows a typical variation of the collector-junction capacitance due to the emitter-bias voltage for a medium frequency ($f_\alpha = 8$ Mc) alloy-junction transistor (2N123). As seen in the graph, with both junctions reverse-biased the capacitance of one junction can be controlled by the bias voltage at the other junction. This phenomenon may be explained qualitatively by the minority carrier distribution within the base region at different emitter-bias voltages (V_{eb}), as shown in Fig. 2(c). Thus, changing V_{eb} from reverse to forward bias causes the width of the emitter-junction depletion layer to vary due to field variation. At the same time, the width of the collector-junction layer is also affected. It is believed that it is mainly due to small changes in the diffusional transfer of thermally-generated minority carriers from the emitter junction to the collector junction. The equivalent circuit in this state is shown in Fig. 2(b). Since the transistor is in the cutoff state, both G_e and G_c are relatively high, and normal minority carrier injection, diffusion, and collection are not taking place.

Although variation of the collector-junction capacity due to the emitter-bias voltage changes in the cutoff state is small, this has some practical significance. With present transistors, which were not designed to be used as variable capacitors, we may not be able to excite the collector-resonance circuit by applying the pump voltage to the emitter, but we are certainly able to lock the phase of the collector oscillation signal (parametrically excited), by applying the phase-lock signal to the emitter junction. Utilizing the above characteristics, a successful parametric-excited resonator was built. A schematic of the experimental circuit is shown in Fig. 3(a). Collector circuit is essentially the parametric-excited resonance circuit tuned to the second subharmonic by collector dc bias-voltage V_{cb}, while the collector-junction capacity is being pumped by V_p at a frequency of 40 Mc. The phase-lock signal (20 Mc) is coupled to the emitter, and V_{eb} biases the emitter junction to the proper operating point.

[1] J. F. Gibbons and G. L. Pearson, "P-N-P variable capacitance diodes," PROC. IRE, vol. 48, pp. 253–255; February, 1960.
[2] J. M. Early, "P-N-P variable capacitance diode theory," PROC. IRE, vol. 48, pp. 1905–1906; November, 1960.
[3] L. J. Giacoletto, "Three-terminal variable capacitance semiconductor device," PROC. IRE, vol. 49, pp. 510–511; February, 1961.
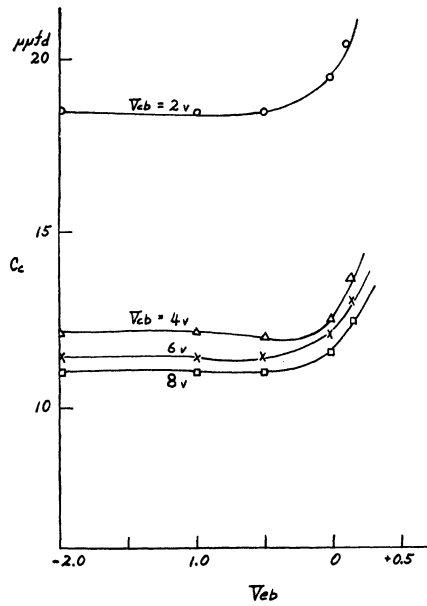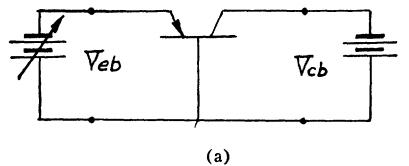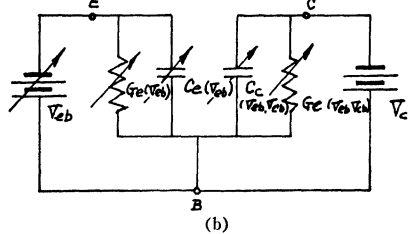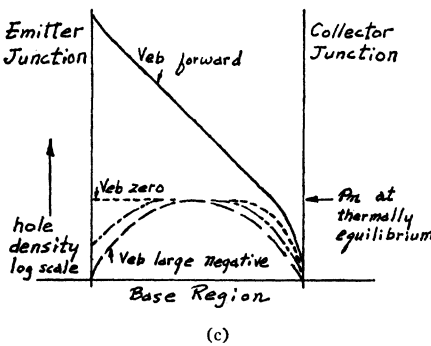

Fig. 1—Collector-junction capacity vs emitter-bias voltage.


(a)

(b)

(c)

Fig. 2—(a) Reverse-biased junction transistor. (b) Equivalent circuit. (c) Minority carrier distribution within base region.

As seen in Fig. 1, in the vicinity of zero emitter bias, the capacitive interaction becomes most significant. But if the emitter should swing into the forward-conduction region, the transistor will become active (normal transistor action), and a relatively large dc current will flow through the collector circuit, damping the oscillation. The signal frequency (20 Mc) current ($\alpha \cdot ie$) due to normal transistor action is negligible because the signal frequency greatly exceeds the α-cutoff frequency of the transistor.
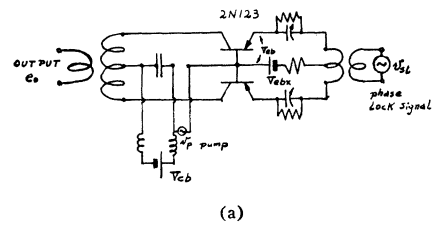
(a)
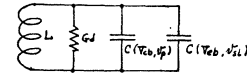
(b)
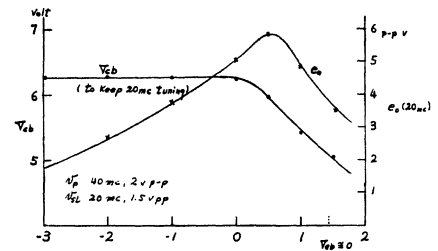
(c)

Fig. 3—Transistor parametric resonator: (a) experimental circuit; (b) equivalent circuit; (c) experimental result.

In Fig. 3(c), output voltage vs emitter dc bias-voltage for a constant drive was plotted. In the same graph, collector-detuning voltage was plotted against the emitter dc bias-voltage for a constant frequency of resonance.

The equivalent circuit of this parametric-excited resonator is shown in Fig. 3(b), and the diode parametric-circuit analysis which was derived by the author or that which was presented by Hilibrand and Beam[4] can be adopted with slight modifications.

The main advantages of this circuit as compared with the conventional diode parametric circuit are: 1) better isolation between input and output due to the use of a three-terminal device; 2) more important, the ability to switch the phase of the output signal without discontinuing the pump signal. The latter fact may be a very significant achievement in the application of the parametric circuit to high-speed phase switching. Because of this, the so-called three-phase pumping system required in the conventional (diode or magnetic core) parametric circuit may be eliminated.

It is well known that the limitations of an ordinary junction transistor in high-frequency applications are mainly due to α-cutoff (diffusion process) and the collector-junction capacity. Utilizing this junction capacity, once regarded as the troublesome factor, in a parametric-excited resonator, we are able to obtain a relatively high gain in the frequency range far beyond the α-cutoff frequency of the junction transistor.

The author is greatly indebted to Prof. Kyhl of MIT for his guidance throughout this work.

YOHAN CHO
EDP Div.
Minneapolis-Honeywell Regulator Co.
Newton, Mass.

[4] J. Hilibrand and W. R. Beam, "Semiconductor diodes in parametric subharmonic generator," RCA Rev., pp. 221–253; June, 1959.

Noise Performance and Stability of a Hybrid-Coupled Tunnel Diode Amplifier*

An interesting hybrid-coupled tunnel diode amplifier has been described recently[1,2] which achieves very wide bandwidth, reasonable gain, low noise, and unconditional stability at the input. Since the performance data supplied by Sie[1] indicate favorable features only, it should be interesting also to recognize facts which limit the actual improvement of the noise performance of a system by using the hybrid-coupled tunnel diode amplifier in the front end of a receiver. This will be explained in the following.

Assume that a generator with an internal conductance G_g, a load G_L, and two equal tunnel diode amplifiers reflecting negative conductance $-G_D$ between the terminals, be properly connected to the hybrid of uniform characteristic conductance G_0. The power reflection coefficient at the hybrid terminals connected to the generator, the load, and the two equal amplifiers with tuned out susceptances are

$$\rho_g = \left(\frac{G_g - G_0}{G_g + G_0}\right)^2 \tag{1a}$$

$$\rho_L = \left(\frac{G_L - G_0}{G_L + G_0}\right)^2 \tag{1b}$$

$$\rho_D = \left(\frac{-G_D + G_1 - G_0}{-G_D + G_1 + G_0}\right)^2, \tag{1c}$$

with G_1 = circuit loss of each tunnel diode amplifier reflected between the hybrid connecting points.

The effective gain of the hybrid amplifier when terminated into the load $G_L = G_0$ is equal to the power reflection at the tunnel diode amplifier terminations:

$$\gamma = \rho_D \tag{2}$$

and the available gain is

$$\gamma_{av} = \gamma(1 - \rho_g) = \rho_D(1 - \rho_g). \tag{3}$$

For the calculation of the noise figure, $G_L = G_0$ is assumed corresponding to $\rho_L = 0$, since this is the interesting condition for unconditional input stability. For the total noise output into $G_L = G_0$ results

$$N_0 = \gamma(1 - \rho_g)kT_gB + \gamma^2\rho_gkT_LB$$
$$+ \frac{4kT_DBG_D'G_0}{(G_0 + G_1 - G_D)^2}(1 + \rho_g\gamma)$$
$$+ \frac{4kT_1BG_1G_0}{(G_0 + G_1 - G_D)^2}(1 + \rho_g\gamma). \tag{4}$$

(T_g, T_L, T_D, T_1 = noise temperatures of generator, load, tunnel diodes and losses.) The first term in this equation is the amplified available generator noise power. The second term is originated by the noise power kT_LB entering the amplifier from the output termination G_L, of which the portion $\gamma^2\rho_g kT_LB$ is delivered back to G_L. The third and fourth terms express the output noise originating from the tunnel diode amplifiers. First, the noise power delivered by each

tunnel diode amplifier into the hybrid may be expressed by

$$N_D + N_1 = \frac{4kT_DBG_D'G_0}{(G_0 + G_1 - G_D)^2}$$
$$+ \frac{4kT_1BG_1G_0}{(G_0 + G_1 - G_D)^2}, \tag{5}$$

with G_D' = effective noise generating conductance of the lossy tunnel diode. Half of this power will go into G_L directly, the other part is directed towards the generator. There a portion of it is reflected back into the hybrid, and subsequently it will appear in the load G_L, multiplied by the factor $\rho_g\gamma$.[3] The same noise power is contributed by the other tunnel diode amplifier. The noise figure that results is:

$$F = \frac{N_0}{\gamma(1 - \rho_g)kT_gB} = 1 + \gamma \frac{\rho_g}{1 - \rho_g} \frac{T_L}{T_g}$$
$$+ \frac{4G_D'G_0(1 + \rho_g\gamma)}{(1 - \rho_g)(G_0 + G_D - G_1)^2} \cdot \frac{T_D}{T_g}$$
$$+ \frac{4G_1G_0(1 + \rho_g\gamma)}{(1 - \rho_g)(G_0 + G_D - G_1)^2} \cdot \frac{T_1}{T_g}. \tag{6}$$

Under ideal conditions, there is no reflection at the input, and any losses in the circuit and the tunnel diodes can be neglected. Then the noise figure becomes:

$$F = 1 + \frac{4G_D/G_0}{(1 + G_D/G_0)^2} \cdot \frac{g_e}{g_D} \cdot \frac{T_D}{T_g}, \tag{7}$$

with $G_D = \eta g_D$, $-g_D$ = negative conductance of the diodes, $g_e = eI_0/2kT_D$, η = transformation factor.

The noise figure is directly related to the gain. From (1c) and (2), one obtains

$$G_D/G_0 = 1 - \frac{2}{\sqrt{\gamma} + 1} \tag{8}$$

and consequently

$$F = 1 + \left(1 - \frac{1}{\gamma}\right)\frac{g_e}{g_D} \cdot \frac{T_D}{T_g}$$
$$= 1 + \left(1 - \frac{1}{\gamma_{av}}\right)\frac{g_e}{g_D} \cdot \frac{T_D}{T_g}$$
$$= 1 + \left(1 - \frac{1}{\gamma_{av}}\right)\frac{eI_0}{2kT_gg_D}. \tag{9}$$

This expression shows that for a given T_g, and diode parameters, the ideal noise figure of the hybrid amplifier depends only on the gain γ, and that the noise figure increases with the gain. The noise figure varies from 1 to a value asymptotically approaching $1 + eI_0/2kT_gg_D$ as the gain is varied from 0 db to large values. The hybrid amplifier shows an improvement by the factor $\gamma_{av} - 1/\gamma_{av}$ compared to the noise of a simple parallel connected tunnel diode amplifier, whose optimal noise figure is $F = 1 + eI_0/2kT_gg_D$ for infinite load impedance. The reason for this improvement is the elimination of the load noise contribution.

The question as to what extent a system is improved using a tunnel diode hybrid preamplifier can be answered as follows: Using

(9), the noise figure of a system becomes

$$F_{system} = F_1 + \frac{F_2 - 1}{\gamma_1}$$
$$= 1 + \frac{g_e}{g_D}\frac{T_D}{T_g} + \frac{F_2 - (1 + g_e/g_DT_D/T_g)}{\gamma_1}. \tag{10}$$

From this the following conclusions are obvious: if the noise figure F_2 of the succeeding stage is greater than $1 + eI_0/2kT_gg_D$, the noise figure of the system can be reduced to this value for $\gamma_1 \to \infty$, ideally. However, if F_2 is smaller than $1 + eI_0/2kT_gg_D$, an improvement of the system is impossible.

Another remark shall concern the stability of the amplifier. If the amplifier is terminated by a load $G_L = G_0$, then with respect to a wave going into the input no wave can ever be reflected, which, at first, means unconditional input stability. However, a stability condition has to be met by the amplifier not only with respect to an incident wave, but also with respect to the varying impedance which appears at the TD amplifier terminals of the hybrid if the generator impedance is varied. This restricts the range of stability, in particular at high gain.

WOLFGANG M. FEIST
Raytheon Co.
Burlington, Mass.
Formerly with
Diamond Ordnance Fuze Labs.
Washington, D. C.

Millimeter-Wave Field-Displacement-Type Isolators with Short Ferrite Strips*

Generally, field-displacement-type isolators have more compact and simple structures than Faraday rotation-type isolators. At millimeter waves this is, however, not always true. For example, the isolator developed by Weiss and Dunn required a ferrite strip length of two inches for 5 mm wavelength.[1] Ayres developed an isolator with a ferrite for 4 mm wavelength with the relatively high magnetic flux density of 12 kilogauss.[2] These long thin ferrite strips break easily.

Recently, field-displacement-type isolators of extremely short ferrite strip (only 0.2 inches) with low magnetic field (less than 5 kilo-oersted) for 5 mm wavelength have been developed by the authors. The ferrite strip was made from a single-crystal-type sample LRR-1 supplied by A. O. Smith Corporation. The sample had an anisotropy field of 18.4 kilo-oersted and a line width of approximately 10 oersted. The sample was magnetized in the direction of easy magnetization.

The ferrite strip of 0.209″×0.0325″ ×0.0117″ was mounted on a polystyrene strip of the same length. This was placed in RG-98/U waveguide as shown in Fig. 1. The external magnetic field was applied parallel to the crystal axis. The magnetic field was applied by an adjustable permanent magnet. This was adjusted for best performance at the operating frequency.

An example of experimentally obtained operating frequency characteristics of this device is shown in Fig. 2. When the operating frequency is changed, the applied magnetic flux density is changed as indicated in the figure. As is well known, the square of the gyromagnetic resonance frequency f_0 can be expressed as a constant coefficient second-order function of the applied magnetic field.[3] If B_0 represents the magnetic flux density in kilo-gauss measured at the air gap where the ferrite strip is mounted when the ferrite resonates, the following equation can be obtained from the experimental data:

$$f_0{}^2 = 30.6B_0{}^2 + 38.1B_0 + 2799 \ (kMc)^2.$$

This equation can help to estimate performance over a wide range of operating frequency and magnetic flux density.
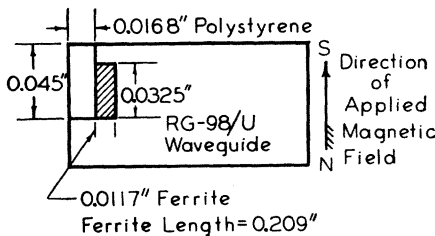

Fig. 1—Cross section of millimeter-wave field-displacement-type isolator.
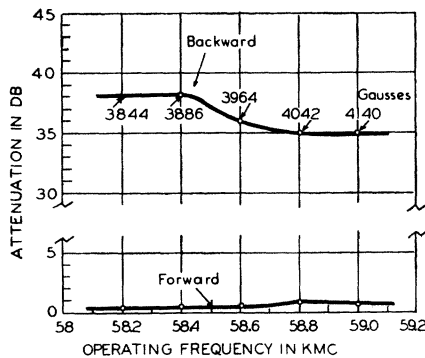

Fig. 2—Operating frequency characteristics of millimeter-wave field-displacement-type isolator.

The frequency bandwidth for 15 db isolation for a fixed magnet adjustment was 190 Mc. The forward attenuation was less than 1 db over the entire band. The frequency bandwidth can be increased by increasing the ferrite strip length. The backward attenuation increased faster than forward attenuation with increasing ferrite strip length.

Even though the mounting position and geometrical shape of the ferrite strip rather

[3] B. Lax, "Frequency and loss characteristics of microwaves ferrite devices," PROC. IRE, vol. 44, pp. 1368–1386; October, 1956.

critically influenced the isolator characteristics, frequency characteristics of the figure of merit of this isolator $F \cong (4\omega/\gamma\Delta H)^2$ were flat for wide range of operating frequencies.[3] The reason is that the line-width ΔH of this material increased linearly with operating frequency. The short strip makes the isolator compact and it makes production easy and inexpensive.

The authors thank A. L. Brault and S. Krupnik for helping with the preparation of the manuscript.

K. Ishii
J. B. Y. Tsui
Dept. Elec. Engrg.
Marquette University
Milwaukee, Wis.
F. F. Y. Wang
Long Range Research
A. O. Smith Corp.
Milwaukee, Wis.

Effect of Filament Magnetic Field on the Electron Beam from a Pierce Gun*

The effect of the magnetic field of a flat, spiral-wound, "noninductive" filament on the electron beam from a shielded Pierce electron gun has been measured by use of a beam tester that has recently been constructed at Cornell University, Ithaca, N. Y. A more detailed report describing the beam tester and other results of tests on dc electron beams will be published in the near future.[1] The beam is produced by a Pierce gun which normally operates at 5400 volts and has a perveance of 1.15×10^{-6}. The cathode diameter is 1.25 inches and the Brillouin beam diameter containing 90 per cent of the beam current is 0.176 inch. The effect of the magnetic field of the filament on the beam shape was determined by taking cross sections, similar to those shown in Fig. 1, along the axis of the beam for filament currents from -7.65 to $+7.65$ amperes. The two beam cross sections shown in Fig. 1 were taken with an x-y recorder. The horizontal and vertical coordinates are the x and y positions in the beam. The deflection above any horizontal line indicates the amount of current collected by a Faraday cage positioned behind a movable plate with a 0.010-inch hole in the center.

The instantaneous filament current was varied while keeping the cathode temperature constant by applying a sinusoidal 60-cps voltage to the filament and by pulsing the cathode at a rate of 60 cps with 16.7-μsec duration pulses. The phase of the cathode pulse relative to the filament voltage was then made variable from $-90°$ to
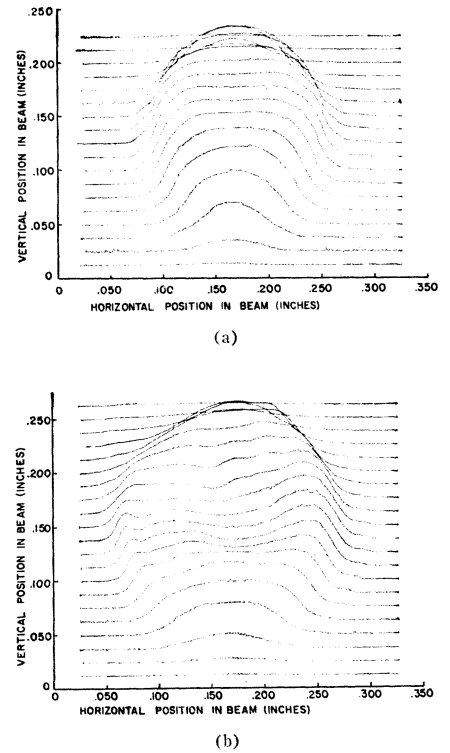
(a)

(b)

Fig. 1—Electron beam cross sections taken with an x-y recorder for (a) Brillouin flow conditions with no current through filament (less than 2 per cent scallop on beam), (b) Brillouin flow conditions with 7.65 amperes through filament.
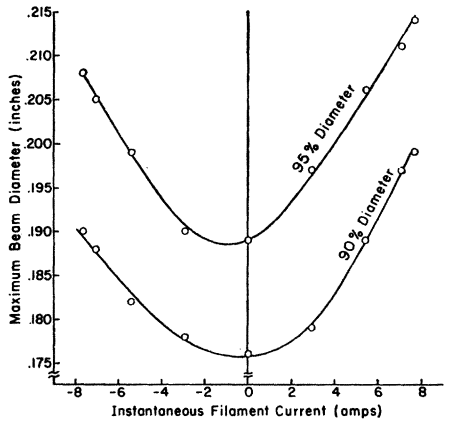

Fig. 2—Maximum beam diameter vs instantaneous filament current.

$+90°$. The curves in Fig. 2 show the maximum beam diameters containing 90 per cent and 95 per cent of the beam current as a function of the current through the filament. Note that the beam diameter obtained when the maximum filament current was present was over 13 per cent greater than that obtained when no filament current was present. In addition to this increase in diameter, a large amount of translaminar current has been noted at all times when the cathode is pulsed while filament current is flowing.

A. S. Gilmour, Jr.
School of Elec. Engrg.
Cornell University
Ithaca, New York